

# Polarization degrees of freedom in photoinduced two-nucleon knockout from finite nuclei

Jan Ryckebusch

*Department of Subatomic and Radiation Physics  
University of Gent, Proeftuinstraat 86, B-9000 Gent, Belgium  
and*

*Institute for Nuclear Theory, University of Washington, Box 351550,  
Seattle, WA 98195*

Dimitri Debruyne and Wim Van Nespen

*Department of Subatomic and Radiation Physics  
University of Gent, Proeftuinstraat 86, B-9000 Gent, Belgium*

(June 8, 2021)

The polarization degrees of freedom in photoinduced two-nucleon knockout from finite nuclei are studied. It is pointed out that they open good perspectives to study the dynamics of dinucleons in the medium in detail. The  $(\gamma, pp)$  and  $(\gamma, pn)$  angular cross sections, photon asymmetries and outgoing nucleon polarizations are calculated for the target nuclei  $^{16}\text{O}$  and  $^{12}\text{C}$  and photonenergies ranging from 100 up to 500 MeV. It is investigated to which degree the two-nucleon emission reaction is dominated by photoabsorption on  $^3S_1(T=0)$  proton-neutron and  $^1S_0(T=1)$  proton-proton pairs in the nuclear medium. The calculations demonstrate that dominance of  $S$  wave photoabsorption in the  $(\gamma, pn)$  channel does not necessarily imply that the reaction mechanism is similar to what is observed in deuteron photodisintegration.

## I. INTRODUCTION

In the late fifties it was pointed out by K. Gottfried that after making a few approximations, the cross section for photoinduced two-nucleon ( $2N$ ) knockout  $\sigma(\gamma, N_a N_b)$  can be related to quantities that are sensitive to the relative and center-of-mass motion of nucleon pairs in the nuclear system [1]. In this pioneering work, it was predicted that  $2N$  knockout cross sections are proportional to the so-called pair function  $F(P)$ , which is related to the probability of finding a nucleon pair with c.m. momentum  $P$  in a finite nuclear system. The c.m. momentum  $P$  can be determined in terms of the momenta of the two escaping nucleons ( $\vec{k}_a$  and  $\vec{k}_b$ ) and the momentum transferred by the photon ( $\vec{q}_\gamma$ ):

$$\vec{P} = \vec{k}_a + \vec{k}_b - \vec{q}_\gamma . \quad (1)$$

It should be noted that as soon as one goes beyond the approximations that are at the basis of the Gottfried approach, the differential cross sections can no longer be formally factorized in terms of the pair function and factors that depend on the relative motion of the active pair. This is for example the case when considering more realistic wave functions than plane waves for the outgoing nucleons. Nevertheless, the dominant role of the pair function  $F(P)$  in the  $A(\gamma, pn)$  and  $A(\gamma, pp)$  processes has been experimentally confirmed [2–5]. This observation raises confidence in that the  $(\gamma, N_a N_b)$  reaction mechanism can be sufficiently kept under control to gain also empirical information about the relative motion of nucleon pairs in the medium. It is worth noting that also the measured  $^{12}\text{C}(e, e'pp)$  [6] and  $^{16}\text{O}(e, e'pp)$  [7] cross sections have recently been shown to scale in terms of the pair function  $F(P)$ .

Pioneering two-nucleon knockout studies with moderate energy resolution were performed at Tokyo and Bonn [8,9]. In recent years, the PIP-TOF collaboration has collected a vast amount of  $2N$  knockout data at the tagged photon facility of the 800 MeV Mainz electron accelerator. In comparison with earlier work, these measurements are characterized by an improved energy resolution and cover a wide photon energy region ( $100 \leq E_\gamma \leq 800$  MeV). Measurements with polarized photon beams on  $^4\text{He}$  and  $^{12}\text{C}$  are in the process of being analyzed. Other experiments with polarized photon beams were performed for the target nuclei  $^3\text{He}$  [10] and  $^{16}\text{O}$  [11] at the LEGS facility located at the Brookhaven National Laboratory. In these experiments, the photon energy ranged from 220 up to 305 MeV. The  $^3\text{He}(\vec{\gamma}, pn)p$  asymmetries turned out to be remarkably similar to those obtained from  $d(\vec{\gamma}, pn)$ , provided that one selects that part in the proton-neutron phase space  $d\Omega_p d\Omega_n dE_p dE_n$  for which the residual proton  $p$  can almost be guaranteed to be at rest. With this restriction, only two nucleons are involved in the reaction process and the residual proton is a spectator. Recently, it was pointed out by Sandorfi and Leidemann [12] that the mere assumption of proton pairs predominantly moving in a relative  $^1S_0$  state has major implications for the linear-polarization  $^3\text{He}(\vec{\gamma}, pp)n$  asymmetries. Along the same lines, Wilhelm, Niskanen and Arenhövel [13] pointed out that relatively simple forms

for the  $(\gamma, pp)$  cross sections and polarization observables can be obtained when assuming photoabsorption on  $^1S_0$  diprotons and dominance of any two of the three multipoles ( $E1, E2, M2$ ) in the transition matrix elements.

Turning to finite nuclei, a number of models to deal with two-nucleon knockout have been developed over the last couple of years. The models fall into different categories. The one developed by the Valencia group [14] aims at describing all the different aspects of the photon-nucleus coupling and pion final-state interactions in a unified diagrammatic approach. This includes all the (multi-)pion and (multi-)nucleon production channels. A very large amount of contributing mechanisms are included in the description of the pion and nucleon photoproduction channels. All this at the expense of the nuclear structure aspects of the reaction which are dealt with in a nuclear-matter approach. The local-density approximation (LDA) is applied to obtain results for finite nuclei. The Valencia calculations have been carefully compared to the  $(\gamma, NN)$  data collected in recent years [15–17]. Generally a fair description of the missing energy spectra is obtained, an exception made for the  $(\gamma, pp)$  channel for which the calculations tend to overestimate the data [15,16]. A major conclusion from these comparisons is that for the photoabsorption mechanism to be two-body in nature one has to select these processes for which the  $A - 2$  fragment is created at low missing energies [4]. At higher missing energies the two-nucleon knockout strength is predicted to be essentially due to initial  $(\gamma, \pi)$  production and subsequent pion final-state interactions. This implies that the higher missing energy range is excluded when studying the properties of dinucleons in the medium. Indeed, in these studies it is essential to guarantee that only two nucleons participate in the reaction process.

The models developed in Pavia [18] and Gent [19] are less ambitious as far as the number of included reaction mechanisms is concerned. They concentrating on the two-body photoabsorption mechanisms and do not include the pion production channels. In the light of the previous discussion, these models are therefore restricted to the low missing energy part of the two-nucleon knockout spectra. In comparison with the Valencia approach, the Gent and Pavia models put more emphasis on a proper description of the nuclear structure aspects of the 2N emission reaction process. In both models, the shell-model framework is the starting point to account for the nuclear structure aspects. In the light of 2N emission processes being a possible probe to study ground-state correlations, the mean-field wave functions are corrected for (central) Jastrow correlation effects.

Here we report on calculations that aim at investigating the dynamics of dinucleons in the medium with the aid of photoinduced two-nucleon knockout. More in particular, we concentrate on the additional degrees of freedom created by using (linearly) polarized photon beams and recoil nucleon polarimetry. The organization of this paper is as follows. In Sect. II the definitions and conventions for the  $(\gamma, NN)$  cross sections and polarization observables are given. Sect. III is devoted to a description of the different assumptions which are at the basis of the model calculations presented here. A factorized (Subsect. III A) and an unfactorized (Subsect. III B) model are sketched. Rather than elaborating on the technical details, we make an attempt to describe the basic ideas and assumptions behind the models. Section IV contains the results of the numerical calculations. We concentrate on proton-proton and proton-neutron knockout from the target nuclei  $^{16}\text{O}$  and  $^{12}\text{C}$  in several kinematical conditions and consider photon energies from 100 up to 500 MeV. Finally, Sect. V contains the conclusions.

## II. DIFFERENTIAL CROSS SECTIONS AND POLARIZATION OBSERVABLES

Using standard techniques the four-fold differential cross section for the photoinduced two-nucleon knockout process  $A + \gamma \longrightarrow A - 2 + N_a + N_b$  in the LAB frame ( $\vec{p}_A = \vec{0}$ ) reads

$$\frac{d^4\sigma}{d\Omega_a d\Omega_b dE_a dE_b} = \frac{1}{(2\pi)^5 E_\gamma} k_a k_b E_b E_a \delta(E_{A-2} + E_a + E_b - E_A - E_\gamma) \overline{\sum_{fi}} |m_F^{fi}(\lambda)|^2, \quad (2)$$

where  $\overline{\sum_{fi}}$  denotes the appropriate averaging over the initial states and sum over the final states. The variables  $k_a$  ( $k_b$ ) and  $E_a$  ( $E_b$ ) refer to the three-momentum and total energy of the escaping nucleons. Further,  $\lambda$  denotes the photon circular polarization. The  $m_F^{fi}(\lambda)$  is the transition matrix element for the reaction under study and is defined as

$$m_F^{fi}(\lambda = \pm 1) = \left\langle \Psi_f^{(A-2)}(E_x, J_R M_R); \vec{k}_a m_{s_a}; \vec{k}_b m_{s_b} \mid J_\lambda(\vec{q}_\gamma) \mid \Psi_0 \right\rangle, \quad (3)$$

where  $|\vec{k}_a m_{s_a}\rangle$  and  $|\vec{k}_b m_{s_b}\rangle$  are the distorted waves of the outgoing nucleon  $N_a$  and  $N_b$  respectively. The  $|\Psi_f^{(A-2)}(E_x, J_R M_R)\rangle$  determines the wave function of the residual  $A - 2$  system. Its excitation energy  $E_x$  is expressed relative to the ground-state energy of the bound  $A - 2$  nucleus. In all forthcoming derivations we assume that the residual nucleus is created in a specific state characterized by an excitation energy  $E_x$  and angular momentum  $J_R$ . This does not imply, however, that our considerations are restricted to the discrete part of the  $A - 2$  spectrum.

Indeed, when the situation occurs that the  $A-2$  nucleus is created in the continuous part of its spectrum a summation over the momenta  $J_R$  has to be carried out.

In all further considerations, the  $z$  axis is chosen along the direction of the incoming photon momentum. The  $xz$  plane is defined by  $\vec{q}_\gamma$  and  $\vec{k}_a$ . The  $y$  axis is then along the direction of the vector  $\vec{q}_\gamma \times \vec{k}_a$ .

The photon asymmetry  $\Sigma$  is given by

$$\Sigma = \frac{d\sigma_{\parallel}(\vec{\gamma}, NN) - d\sigma_{\perp}(\vec{\gamma}, NN)}{d\sigma_{\parallel}(\vec{\gamma}, NN) + d\sigma_{\perp}(\vec{\gamma}, NN)}, \quad (4)$$

where  $d\sigma_{\parallel(\perp)}$  is the differential cross section for photons linearly polarized parallel (perpendicular) to the  $xz$  reaction plane. The polarization for the nucleon  $N_a$  is defined according to

$$P_y^a = \frac{d\sigma^{\uparrow}(\gamma, \vec{N}_a N) - d\sigma^{\downarrow}(\gamma, \vec{N}_a N)}{d\sigma^{\uparrow}(\gamma, \vec{N}_a N) + d\sigma^{\downarrow}(\gamma, \vec{N}_a N)}, \quad (5)$$

where  $d\sigma^{\uparrow(\downarrow)}$  is the differential cross section for nucleon  $N_a$  polarized along (against) the  $y$ -axis. Remark that the choice of the reference system is such that the nucleon on which recoiling nucleon polarimetry is performed is labelled as  $N_a$  and that the spin is measured along the direction normal to the reaction plane containing  $\vec{q}_\gamma$  and  $\vec{k}_a$ .

The unpolarized differential cross section and asymmetry can be written in terms of structure functions and read [20]

$$\frac{d^4\sigma}{d\Omega_a d\Omega_b dE_a dE_b} = \frac{1}{(2\pi)^5 E_\gamma} k_a k_b E_b E_a \delta(E_{A-2} + E_a + E_b - E_A - E_\gamma) \frac{1}{2} W_T \quad (6)$$

$$\Sigma = -\frac{W_{TT}}{W_T}, \quad (7)$$

with

$$W_T(q_\gamma, k_a, k_b, \theta_a, \theta_b, \phi_a, \phi_b) = \sum_{m_{s_a}, m_{s_b}, M_R} \left[ \left( m_F^i(\lambda = +1) \right)^* \left( m_F^i(\lambda = +1) \right) + \left( m_F^i(\lambda = -1) \right)^* \left( m_F^i(\lambda = -1) \right) \right] \quad (8)$$

$$W_{TT}(q_\gamma, k_a, k_b, \theta_a, \theta_b, \phi_a, \phi_b) = 2Re \left[ \sum_{m_{s_a}, m_{s_b}, M_R} \left( m_F^i(\lambda = -1) \right)^* \left( m_F^i(\lambda = +1) \right) \right]. \quad (9)$$

At this point it is worth remarking that the unpolarized ( $e, e' N_a N_b$ ) cross section depends on both the  $W_T$  and  $W_{TT}$  structure function. Apart from these, the ( $e, e' N_a N_b$ ) differential cross section is further determined by the  $W_{LT}$  and  $W_L$  structure function, reflecting the longitudinal degree of freedom in electron scattering. In any case, with the aid of polarized real photon beams one can gain control over the transverse channels which have been shown to contribute substantially to triple coincidence reactions of the ( $e, e' N_a N_b$ ) type [21,22].

The outgoing nucleon polarization can be written in the following form

$$P_y^a = \frac{1}{W_T} \sum_{m_{s_b}, M_R, \lambda \pm 1} Re \left[ i \left\langle \Psi_f^{(A-2)}(E_x, J_R M_R); \vec{k}_a m_{s_a} = 1/2; \vec{k}_b m_{s_b} \mid J_\lambda(\vec{q}) \mid \Psi_0 \right\rangle \times \left\langle \Psi_f^{(A-2)}(E_x, J_R M_R); \vec{k}_a m_{s_a} = -1/2; \vec{k}_b m_{s_b} \mid J_\lambda(\vec{q}) \mid \Psi_0 \right\rangle^* \right]. \quad (10)$$

### III. MODELS FOR EXCLUSIVE TWO-NUCLEON KNOCKOUT FROM FINITE NUCLEI

Direct two-nucleon knockout following photoabsorption is dominated by two-body current operators  $J_\lambda^{[2]}(\vec{q})$ . In our model calculations, an effective Lagrangian approach is adopted to construct the two-body currents that determine the coupling of the photon field to the nuclear system. In selecting the current operators or, equivalently, the contributing reaction mechanisms, we have been led by the observation that the dominant role of (virtual) pion production in

photoinduced two-nucleon knockout has been established in several photoabsorption calculations [14,23,24]. The most elementary process that allows gaining control over the role of the pion in photoinduced experiments is pion photoproduction on the nucleon  $\gamma + N \rightarrow N' + \pi$ . It is very well known that for photonenergies below 0.5 GeV the cross sections and polarization observables for these reactions are fairly well understood in an effective Lagrangian approach retaining a selected class of diagrams [25,26]. The diagrams which are commonly included in photopion production studies are shown in Fig. 1. We now transfer all elementary pion production processes of Fig. 1 to the nuclear medium and assume that the created pion is reabsorbed. As a result of such a process a second nucleon can be brought on the mass shell and one obtains the diagrams of Fig. 2 all feeding the two-nucleon knockout channel. These diagrams represent the processes which are believed to be the major contributors to the  $(\gamma, NN)$  reaction process at low missing energies. In Figure 2, diagrams (a), (b), (d) and (e) correspond with genuine two-body photoabsorption, respectively related to meson-exchange ((a) and (b)) and isobaric currents ((d) and (e)). Diagrams (c) and (f) are characterized by one-body photoabsorption with subsequent two-nucleon knockout and refer to final-state interactions and ground-state correlations respectively.

The two-body operators related to Fig. 2(a) and (b) are the standard pion-exchange current operators that can be derived from the one-pion exchange part of the nucleon-nucleon interaction through minimal substitution [25,27]. We use the standard  $\pi NN$  pseudo-vector coupling with  $f_{\pi NN}^2/4\pi = 0.079$  and regularize the  $\pi NN$  vertices with monopole form factors using a cut-off mass of  $\Lambda_{\pi NN} = 1200 \text{ MeV}$ . The one-nucleon photoabsorption mechanism of Figure 2(f) would not contribute in a shell-model (or independent particle) picture of the target nucleus and refers to the situation in which one-body photoabsorption on a correlated pair forces two nucleons to escape. In principle, this process could be treated on the same footing as the other contributing diagrams. This would imply, however, that solely ground-state correlations induced by the one-pion exchange part of the nucleon-nucleon interaction are included. This is at odds with the widely spread belief that heavier meson exchange is the major source of ground-state correlations. Generally, short-range effects are difficult to deal with in a diagrammatic approach. Nevertheless, various techniques have been developed to cope with the complexity of the ground-state of an interacting Fermion system. Here, we resort to a semi-phenomenological approach to relate the results of these theoretical ground-state investigations with the cross sections and polarization observables for  $(\gamma, NN)$  reactions. It consists of correcting the mean-field Slater determinant  $|\Psi_o\rangle$  with a Jastrow-like correlation function :

$$\prod_{i<j} f_c(r_{ij}) |\Psi_o\rangle . \quad (11)$$

Such an expansion mocks up two-, three-, ... A-body correlations. In the actual calculations only the central correlations of the two-body type are retained. As a matter of fact, such an approximation amounts to correcting the product of the single-particle bound-state functions of the active nucleon-pair  $\phi_a(1)\phi_b(2)$  with a central correlation function :

$$\phi_a(1)\phi_b(2) \rightarrow \phi_a(1)\phi_b(2)f_c(r_{12}) . \quad (12)$$

In an attempt to find out about the sensitivity of the  $(\gamma, NN)$  angular cross sections and polarization observables to the ground-state correlations we have used several types of correlation functions in the calculations.

The results of this paper will confirm the importance of the  $\Delta_{33}$  resonance in photoinduced two-nucleon knockout for photonenergies below 0.5 GeV. As we consider photon energies in the resonance region special care must be taken in constructing the isobaric current operators related to intermediate  $\Delta_{33}$  creation of the type  $\gamma NN \rightarrow N\Delta \rightarrow NN$ . A detailed account of the isobaric currents in the context of two-nucleon knockout reactions was given in Ref. [22]. As our model calculations start from the assumption that the pion is the major mediator between several nucleons, the  $V_{NN,N\Delta}$  interaction which enters in the construction of the isobaric currents is the pion exchange interaction.

### A. A factorized model for photoinduced two-proton knockout

We now consider a simplified model for  $(\gamma, N_a N_b)$ . Two approximations are necessary for the angular  $(\gamma, NN)$  cross section to factorize. First, a plane wave description for the escaping particles should be adopted. In addition, a severe assumption regarding the relative motion of the pairs has to be made in the sense that the decoupling of the c.m. and relative motion of the pair can formally only be achieved after the photon is assumed to couple to dinucleons residing in relative  $S$  waves. This simplification is known as the ‘‘quasi-deuteron’’ approximation. This terminology might be a bit confusing in the sense that is used for both proton-proton and proton-neutron knockout. Furthermore, the range of the relative  $S$  wave is assumed to be small in comparison with all other mechanisms that play a role in the reaction process. From the technical point of view, this allows replacing the relative  $S$  wave by a

delta function (known as the “zero-range approximation”), thus enormously simplifying the theoretical calculations [28–31]. The “zero-range approximation” somehow implies that one simplifies the Fermi motion in the relative wave function of the pair. The factorized scheme can be equally well applied to  $(\gamma, pn)$  and  $(\gamma, pp)$  reactions. The fact that solely the terms related to the ground-state correlations and a few pieces from the isobaric current contribute to the direct proton-proton knockout mechanism makes the factorized model to be particularly attractive as rather simple analytical expressions for the asymmetry and cross sections can be derived. The procedure for arriving at factorized expressions for the structure functions was outlined in Ref. [30]. For the sake of completeness we rewrite the derived expressions for the  $W_T$  and  $W_{TT}$  structure functions at the real photon point

$$\begin{aligned}
W_T &= F_{hh'}(P) \left\{ \frac{\mu_p^2 e^2 q_\gamma^2}{M_p^2} (g(k_+) - g(k_-))^2 \right. \\
&\quad + \frac{e^2}{2M_p^2} \left[ (k_{a,x}g(k_-) + k_{b,x}g(k_+))^2 + (k_{a,y}g(k_-) + k_{b,y}g(k_+))^2 \right] \\
&\quad + \frac{256}{81} \left( \frac{f_{\gamma N \Delta} f_{\pi N \Delta} f_{\pi NN}}{m_\pi^3} \right)^2 G_\Delta^2 \left( \vec{q}_\gamma \times \left( \frac{\vec{k}_a - \vec{k}_b}{2} \right) \right)^2 \times \left[ \vec{k}_+ \frac{1}{k_+^2 + m_\pi^2} - \vec{k}_- \frac{1}{k_-^2 + m_\pi^2} \right]^2 \Big\} \\
W_{TT} &= F_{hh'}(P) \left\{ \frac{-2\mu_p^2 e^2 q_\gamma^2}{M_p^2} (g(k_+) - g(k_-))^2 \right. \\
&\quad - \frac{e^2}{M_p^2} \left[ (k_{a,x}g(k_-) + k_{b,x}g(k_+))^2 - (k_{a,y}g(k_-) + k_{b,y}g(k_+))^2 \right] \\
&\quad - \frac{256}{81} \left( \frac{f_{\gamma N \Delta} f_{\pi N \Delta} f_{\pi NN}}{m_\pi^3} \right)^2 G_\Delta^2 \left[ \left( \vec{q}_\gamma \times \left( \frac{\vec{k}_a - \vec{k}_b}{2} \right) \right)_x^2 - \left( \vec{q}_\gamma \times \left( \frac{\vec{k}_a - \vec{k}_b}{2} \right) \right)_y^2 \right] \\
&\quad \times \left[ \vec{k}_+ \frac{1}{k_+^2 + m_\pi^2} - \vec{k}_- \frac{1}{k_-^2 + m_\pi^2} \right]^2 \Big\}, \tag{13}
\end{aligned}$$

with

$$\vec{k}_\pm = \frac{\vec{k}_a - \vec{k}_b}{2} \pm \frac{\vec{q}_\gamma}{2}. \tag{14}$$

The function  $g(k)$  appearing in the above expression is the Fourier transform of the central correlation function

$$g(k) \equiv \int d\vec{r} e^{i\vec{k}\cdot\vec{r}} (1 - f_c(r)), \tag{15}$$

and  $F_{hh'}(P)$  is the probability of finding a proton pair with quantum numbers  $(h(n_h l_h j_h), h'(n_h l_h j_h))$ , c.m. momentum  $P$  and small internucleon separations in the target nucleus. The  $G_\Delta$  is the sum of the “resonant” (direct  $\Delta$  term corresponding with Fig.2(d)) and non-resonant  $\Delta$  propagator (crossed  $\Delta$  term corresponding with Fig.2(e)).

$$\begin{aligned}
G_\Delta &\equiv G_\Delta^{res} + G_\Delta^{non-res} \\
&= \frac{1}{-E_\Delta^{res} + M_\Delta - \frac{i}{2}\Gamma_\Delta^{res} + V_\Delta} + \frac{1}{-E_\Delta^{non-res} + M_\Delta}, \tag{16}
\end{aligned}$$

where  $M_\Delta = 1232$  MeV,  $\Gamma_\Delta^{res}$  is the free  $\pi N$  decay width and  $V_\Delta$  is the  $\Delta$  selfenergy in the medium. For light nuclei the imaginary part of this selfenergy is established to be 40 MeV at full nuclear density [25,32]. The  $E_\Delta^{res}$  and  $E_\Delta^{non-res}$  are the invariant energies of the  $\Delta$  in respectively the diagram of Fig. 2(d) and (e). In deriving the analytical expressions of Eq.(13) the  $\Delta$ -current terms in  $(G_\Delta^{res} - G_\Delta^{non-res})$  have been neglected.

The first two terms in the expressions for  $W_T$  and  $W_{TT}$  refer to one-body photoabsorption on the magnetization and convection current respectively. Retaining only the contribution from  $\Delta$  current to the above structure functions and using the identity (7) one readily obtains the following expression for the  $(\gamma, pp)$  asymmetry

$$\Sigma = - \frac{k_a^2 \sin^2 \theta_a \cos 2\phi_a + k_b^2 \sin^2 \theta_b \cos 2\phi_b - 2k_a k_b \sin \theta_a \sin \theta_b \cos(\phi_a + \phi_b)}{k_a^2 \sin^2 \theta_a + k_b^2 \sin^2 \theta_b - 2k_a k_b \sin \theta_a \sin \theta_b \cos(\phi_a - \phi_b)}, \tag{17}$$

where  $(\theta, \phi)$  are the polar and azimuthal angle of the escaping nucleons. For planar kinematics the isobar contribution to  $W_T$  and  $W_{TT}$  is equal and in the absence of ground-state correlations the factorized model predicts that the  $(\vec{\gamma}, pp)$  asymmetry is exactly -1. At first sight this conclusion seems to be at odds with the fact that symmetry observations require  $\Sigma = 0$  for  $\theta_1, \theta_2 \in \{0^\circ, 180^\circ\}$ . Under these circumstances, however, also the  $\Delta$  current contributions to the  $W_T$  and  $W_{TT}$  structure functions are predicted to be exactly zero for both photon polarizations, leaving the photon asymmetry  $\Sigma$  undetermined. Remark that the major contribution from the ground-state correlations, namely the one originating from photoabsorption on the one-body magnetization current [30], does equally contribute to  $W_T$  and  $W_{TT}$ . Moreover, in both cases it has the same relative sign with respect to the isobaric terms. For that reason the factorized scheme suggests that no particular sensitivity of the  $(\gamma, pp)$  asymmetries to ground-state correlations should be expected. The above expression further suggests a sort of universal behaviour for the asymmetry of direct  $(\gamma, pp)$  processes, which is independent from the shell-model structure of the active pair or target mass number  $A$  and only involves the momenta of the two ejected protons. We did not succeed in deriving a simple form for the  $P_y^p$ . In order to reach scaling in terms of the pair function  $F(P)$  one relies on closure properties and such a procedure seems to be excluded when nucleon spin observables are probed.

## B. Unfactorized model for photoinduced $2N$ knockout

In Refs. [19,22] an unfactorized model for calculating two-nucleon knockout cross sections was presented. In comparison with the factorized model outlined in previous Subsection it provides a more realistic description of the escaping nucleon wave functions. Moreover, no assumptions are made regarding the nature of the relative wave function of the active nucleon pair. As a matter of fact, the unfactorized model does not make the separation between relative and center-of-mass motion as this can only be achieved in a harmonic oscillator basis. Instead of working in a harmonic oscillator basis, we use mean-field quantities (wave functions, potentials and phase shifts) from a Hartree-Fock calculation with the effective Skyrme force SkE2 [33]. We deem these single-particle wave functions to be realistic, as we could obtain a good description for the exclusive quasi-elastic  $(e, e'p)$  cross sections using these wave functions and modern optical potentials [34]. Here, we solely summarize the physical ideas behind the unfactorized model and refer to Refs. [19,22] for the technical details. The principal idea is that following the absorption of a photon by the target nucleus, two nucleons are excited from a bound into a continuum eigenstate of a mean-field potential. By making a proper partial wave expansion with products of these continuum eigenstates, an antisymmetrized wave function can be constructed that is characterized by two asymptotically escaping nucleons and a residual  $A - 2$  fragment. In order to ensure the antisymmetrization of the final wave function we found it appropriate to start from a basis set in which the residual fragment is created with a particular angular momentum  $J_R$ . Within the outlined approach, the essential quantities that enter the calculation of the two-nucleon knockout cross sections are the reduced transition matrix elements of the type

$$\langle p(\epsilon l j) p'(\epsilon' l' j'); J_1 \| T_J(q_\gamma) \| h(n_h l_h j_h) h'(n_{h'} l_{h'} j_{h'}); J_R \rangle, \quad (18)$$

where  $h$  ( $h'$ ) are the bound state wave functions for the orbits from which the nucleons are escaping and  $p$  ( $p'$ ) the continuum eigenfunctions of the mean-field potential. The  $T_J$  stands for the magnetic and electric transition operator which is obtained after making a multipole decomposition of the current operators. For the results presented here we reached convergence after including all electric and magnetic multipoles up to  $J=5$ . Each of the diagrams of Figure 2 will contribute to the transition operator  $T_J$ . For the meson-exchange and isobaric currents the expressions for the matrix elements are given in the Appendix of Ref. [19]. It should be noted that in the latter reference, which concentrated on photonenergies below the resonance region, the static limit for the  $\Delta$  propagators were considered. Here an updated version that uses dynamic  $\Delta$  propagators and accounts for both the direct and crossed  $\Delta$  terms has been used. The corresponding current operator was described in detail in Refs. [22,31]. This current operator could fairly well describe the photon energy dependence of the  $^{12}\text{C}(\gamma, pn)$  and  $^{12}\text{C}(\gamma, pp)$  cross sections through the  $\Delta$  resonance region [35]. The procedure for including the ground-state correlation effects of Figure 2(f) was outlined in Ref. [22], where also the expression for the corresponding reduced matrix elements are given. We would like to stress that the unfactorized model can be used with plane wave outgoing nucleon waves. It suffices to use Bessel functions for the continuum single-particle states  $p(\epsilon l j)$  and  $p'(\epsilon' l' j')$  in the above matrix element. The fact that the same Hamiltonian is used to construct the mean-field and the bound-state wave functions, together with the transverse nature of the isobaric current, makes the  $(\gamma, pp)$  calculations gauge invariant.

## IV. RESULTS AND DISCUSSION

In what follows, predictions for  $^{16}\text{O}$  and  $^{12}\text{C}(\gamma, NN)$  differential cross sections and polarization observables will be presented. The sensitivity of the measurable quantities to the various aspects of the reaction mechanism will be discussed. The role of the final state interaction can be assessed by considering that the unfactorized model can be applied with either distorted or plane wave outgoing nucleon wave functions, keeping all other ingredients of the calculations exactly equal. The extent to which proton-proton knockout is dominated by  $S$  wave absorption, will be estimated by comparing the results obtained within the context of the full unfactorized model with the predictions from the factorized scheme. Indeed, the latter model is explicitly based on the dominance of  $^1S_0$  proton pairs whereas no such restrictions are made for the unfactorized approach. In the course of this section we will suggest another way of gaining insight into the role of the different combinations for the relative wave function in the photoabsorption mechanism. The method is based on the selective nature of the photoabsorption mechanism when the final state is created with a specific angular momentum  $J_R$ .

The reason for concentrating on p-shell nuclei is partly inspired by the observation that the bulk of the experimental activities are concentrated in this part of the mass table. For the heavier target nuclei the transparency, which is related to the probability for nucleons to escape, is considerably smaller [36]. Accordingly, the ambiguities with respect to the FSI in two-nucleon emission reactions are expected to become increasingly worrying with increasing target mass number  $A$ .

We consider two types of kinematical conditions that create favourable conditions to study the dynamics of pairs in the medium and present exclusive cross sections for (groups of) states in the low missing-energy range.

### A. $^{16}\text{O}(\gamma, NN)$ and $^{12}\text{C}(\gamma, NN)$ in quasi-deuteron kinematics

In this Subsection we are presenting cross sections in so-called ‘‘quasi-deuteron’’ (QD) kinematics which is constrained by imposing the condition that the missing momentum  $|\vec{P}|$  equals zero. Accordingly, one is considering photoabsorption on dinucleons which are at rest (this of course in an ideal world in which final state interactions could be completely ignored). For in-plane kinematics, the QD condition leads to a unique solution for  $\theta_b$ ,  $|\vec{k}_a|$  and  $|\vec{k}_b|$  for each given set of  $(\vec{q}_\gamma, \theta_a, E_x)$ . The effect of the c.m. motion on the angular cross sections is then minimized as the pair function  $F(P=0)$  remains constant. Accordingly it is hoped that a maximized sensitivity to the dynamics of the pair relative motion can be achieved. Quasi-deuteron kinematics further allows comparing  $A(\gamma, pn)$  observables with results obtained in photodisintegration of the deuteron. This opens perspectives to study in how far proton-neutron pairs in the medium resemble quasi-deuteron properties and to learn more about possible medium modifications of the photon-nucleus coupling. From the experimental point of view QD kinematics has the obvious advantage of sampling that region of the phase space for which the largest cross sections are expected.

It is worth reminding that we have used realistic single-particle wave functions in our calculations and do not rely on an expansion in terms of relative and c.m. Harmonic-Oscillator wave functions in order to calculate the cross sections. Nevertheless, it turns out that considering the different relative and c.m. combinations in the Harmonic Oscillator limit is very helpful in interpreting the general behaviour of the angular cross sections and polarization observables. In Tables I and II we have collected all the possible quantumnumbers of the pair relative and c.m. wave functions for proton-proton and proton-neutron knockout from the different s- and p-shell combinations. The combinations are made as if the bound state wave functions are of the simple Harmonic-Oscillator type. After making a separation in the relative and c.m. motion through a Moshinsky transformation the antisymmetric two-body wave functions read

$$\begin{aligned}
 |(n_a l_a j_a t_a, n_b l_b j_b t_b); J_R M_R\rangle_{as} &= \sum_{LM_L} \sum_{nl} \sum_{N\Lambda} \sum_{SM_S} \sum_{TM_T} \hat{j}_a \hat{j}_b \hat{L} \hat{S} \left\langle \frac{1}{2} t_a \frac{1}{2} t_b \mid T M_T \right\rangle \\
 &\times \langle L M_L S M_S \mid J_R M_R \rangle \left\{ \begin{array}{c} l_a \ l_b \ L \\ \frac{1}{2} \ \frac{1}{2} \ S \\ j_a \ j_b \ J_R \end{array} \right\} \langle nl, N\Lambda; L \mid n_a l_a, n_b l_b; L \rangle \\
 &\times \left| (nl, N\Lambda) LM_L, \left( \frac{1}{2} \ \frac{1}{2} \right) SM_S, \left( \frac{1}{2} \ \frac{1}{2} \right) TM_T \right\rangle [1 - (-1)^{l+S+T}] , \tag{19}
 \end{aligned}$$

where  $\hat{j} \equiv \sqrt{2j+1}$ ,  $T(S)$  is the total isospin (spin) of the pair and  $l(\Lambda)$  the angular momentum of the relative (c.m.) pair wave function. In the above expression we have used the conventions of Ref. [37] for the angular momentum coupling coefficients. For direct two-nucleon knockout from a  $0^+$  target nucleus the *total* angular momentum of the pair (which is the sum of the c.m. angular momentum, relative angular momentum and total spin of the pair)

determines the quantum number  $J_R$  of the residual fragment. By studying the cross section for the different  $J_R$ 's, which could experimentally be achieved in a high-resolution experiment [7,38], one can then study the behaviour of the observables as a function of the various types of relative pair wave functions. In QD kinematics, pair c.m. wavefunctions with an angular momentum  $\Lambda > 0$  are unlikely to contribute substantially to the differential cross sections. Assuming that the initial photoabsorption occurs on a relative  $S$  state, then knockout from the  $(1p_{3/2})^2$  configuration is expected to populate a  $J_R = 0^+$  (proton-proton case) and  $J_R = 1^+$  (proton-neutron case). We have calculated the observables for proton-proton and proton-neutron knockout from  $^{12}\text{C}$  considering QD kinematics and four representative photon energies. The results are summarized in Figs. 3 and 4 and refer to the situation in which the  $A - 2$  fragments  $^{10}\text{B}$  and  $^{10}\text{Be}$  are created in a  $(1p_{3/2})^{-2}$  two-hole state. The figures show the contribution for the individual angular momentum components  $J_R$  of the  $A-2$  fragment as well as the result (solid lines) which is obtained after incoherently adding all the components. Accordingly, the solid lines reflect the situation in which an integration over the missing-energy range for p-shell knockout would be made.

The results of Figs. 3 and 4 are in conformity with the above predictions in the sense that the major contribution to the respective cross sections comes indeed from  $J_R=0^+$  (proton-proton case) and  $J_R=1^+$  (proton-neutron case). These are the states that one would expect to be populated assuming absorption on dinucleons in relative  $S$  waves and c.m. angular momentum  $\Lambda=0$ . The latter type of components are naturally favoured in QD kinematics. Nevertheless, the calculations produce substantial contributions from configurations that fall beyond this QD picture. The population of the  $0^+$  state in the  $(\gamma, pn)$  reaction with a non-negligible cross section could be interpreted as a manifestation of photoabsorption on  $^1S_0(T)=1$  proton-neutron pairs which is a slightly unbound configuration in the free proton-neutron system. The next two important  $J_R$ 's contributing to the  $(\gamma, pn)$  observables are  $J_R = 0^+$  and  $3^+$ . The  $J_R = 2^+$  cross section is very small. It should be stressed that all above statements regarding the relative population of the states apply to QD kinematics and should not be considered as general. When moderate and larger values of the missing momentum  $P$  are probed, configurations with c.m. angular momenta  $\Lambda > 0$  are expected to start playing a major role and the relative population of the different angular momentum states of the  $A - 2$  fragment is expected to be different. Moving out of QD kinematics is expected to make the role of the c.m. configurations with  $\Lambda > 0$  more important. At the same time, the cross sections will become smaller as larger values of the missing momentum are probed.

When comparing the corresponding proton-proton and proton-neutron results of Figs. 3 and 4 one observes that the  $(\gamma, pn)$  asymmetries are generally smaller than the  $(\gamma, pp)$  ones. A similar remark holds for the polarizations. It is also worth remarking that the shapes of the proton-proton and proton-neutron differential cross sections are considerably different at corresponding photon energies. The angular dependency and magnitude of the polarization observables is noticed to be remarkably close to the ones for the  $J_R = 0^+$  ( $(\gamma, pp)$ ) and  $J_R = 1^+$  ( $(\gamma, pn)$ ) component. Even more than the cross sections the polarization observables seem to be dominated by photoabsorption on  $(l = 0, \Lambda = 0)$  pairs in QD kinematics. This seems to be particularly the case for the higher end of the photon energies considered here and is more pronounced in the  $(\gamma, pn)$  channel. In an attempt to investigate whether  $S$  wave absorption automatically implies that the  $(\gamma, pn)$  observables exhibit a deuteron like behaviour we have compared the  $^{12}\text{C}(\gamma, pn)$  asymmetries with  $d(\vec{\gamma}, p)n$  data at corresponding photon energies. At  $E_\gamma=100$  MeV the deuteron asymmetry has very little resemblance with the  $^{12}\text{C}$  predictions. This points towards different underlying reaction mechanisms. Whereas, one-body photoabsorption plays an important role for the  $d(\gamma, p)n$  observables at low photon energies [40,41], the calculations predict that  $^{12}\text{C}(\gamma, pn)$  is dominated by pion exchange currents. As one moves into the  $\Delta$  resonance region, the calculated  $^{12}\text{C}$  asymmetries move closer to the deuteron data. At  $E_\gamma=300$  and 400 MeV the agreement of the  $^{12}\text{C}$  asymmetries with the deuteron data is even remarkable. At these energies, also the  $^{12}\text{C}$  proton polarizations  $P_y^p$  turn out to have the same sign and similar magnitude than what was obtained in  $d(\gamma, \vec{p})n$  measurements.

We now investigate the sensitivity of the  $(\gamma, pn)$  observables to the different ingredients which enter the calculations. Fig. 5 shows the calculated  $^{16}\text{O}(\gamma, pn)$  results for  $E_\gamma=150$  MeV in QD kinematics. We consider the situation whereby the two nucleons are emitted from the  $1p$  shell. Two different types of shell-model configurations were considered:  $(1p_{3/2})^{-2}$  and  $(1p_{3/2})^{-1}(1p_{1/2})^{-1}$ . To obtain the curves of Fig. 5 the contributions from the  $J_R$  components to the various cross sections ( $\sigma, \sigma^\uparrow, \sigma^\downarrow, \sigma_\parallel, \sigma_\perp$ ) were incoherently added. The sensitivity to the various terms in the photoabsorption process is illustrated by comparing the dashed and dotted line. Relative to a calculation that solely accounts for the seagull pion-exchange diagram (Fig. 2(a)), the inclusion of the pion-in-flight term (Fig. 2(b)) reduces the cross section and does even switch the sign of the asymmetry. This illustrates the sensitivity of the latter to the different contributing terms in the pion exchange part of the photoabsorption mechanism. Remark that even at photonenergies as low as 150 MeV the effects from the isobaric current are sizeable. The dot-dashed line uses the full photoabsorption operator but plane waves for the escaping proton and neutron wave function. Comparing these results with the solid line, which is obtained with exactly the same current operator but using distorted outgoing nucleon waves, one can estimate the role of the final-state interaction. The asymmetry is hardly affected by the outgoing nucleon distortions, whereas the differential cross section is roughly reduced by a factor of two. The effect



of the distortions on the proton polarizations is large. Its magnitude is of the same order as the deuteron results at corresponding photon energies [39–41]. In comparing the  $(\gamma, pn)$  results of Fig. 5 for both shell-model configurations one gets a feeling about the nuclear structure dependency of the cross sections and polarization observables. In this context it is worth remarking that in the Hartree-Fock basis that we are using the radial dependence of the  $1p_{3/2}$  and  $1p_{1/2}$  single-particle wave functions differs. The general trends for all observables are rather uniform for both configurations. The subtle differences between the two situations are mainly a manifestation for the importance of mechanisms that go beyond  ${}^3S_1$  absorption. Indeed if there would be solely quasi-deuteron like absorption on  $({}^3S_1(T=0), \Lambda=0)$  pairs both shell-model configurations would be dominated by the  $J_R=1^+$  contribution.

Predictions for the  ${}^{12}\text{C}(\gamma, pp)$  cross section within the simple factorized model are shown in Fig. 6 and are compared with the full (unfactorized) model calculations. At low photon energies, where the range of the photons is really too large to expect mere photoabsorption on short-ranged  $S$ -waves, the factorized model largely undershoots the full model calculations. With increasing photon energy, the factorized predictions seem to get closer to the full model predictions. The full model calculations, however, produce differential cross sections which are not as sharply peaked. Referring to the results of Fig. 3, which shows the different  $J_R$  contributions for the distorted wave (solid line) calculation of Fig. 6, this is mainly due to excitation of the  $J_R=1^+$  state, which is somehow excluded when considering  $({}^1S_0, \Lambda=0)$  “quasi-deuteron” absorption. Remark further that the proton angle dependence for the  $J_R=0^+$  contribution in the unfactorized model (Fig. 3), which is the configuration that dominant  $S$ -wave photoabsorption would select, bears a strong resemblance with the factorized model’s prediction. As a consequence, it can be concluded that a major source of deviations between the results produced by the factorized scheme and the full model calculations has to be ascribed to photoabsorption mechanisms that go beyond a quasi-deuteron like mechanism. The effect of the final state interaction can be estimated by comparing the solid and dashed line in Fig. 6. As is usually the case, the final-state distortions tend to widen the peaks of the angular cross sections obtained in the plane-wave approximation. The effect of the outgoing nucleon distortion is particularly large for the left panel of Fig. 6. The typical outgoing nucleon kinetic energy is 20-50 MeV, which makes this result not that surprising. Remark that for this low photonenergy the effect of the FSI on the  $\Sigma$  is even sizeable. For the right panel, corresponding with outgoing nucleon kinetic energies ranging from 60-210 MeV, the role of the outgoing nucleon distortions is minor but not negligible.

A plane wave calculation with a Hermitian current operator would produce an outgoing nucleon polarization which is exactly zero. Two mechanisms of completely different origin can make  $P_y^p$  different from zero. First, final state interaction effects and secondly, the fact that the  $\Delta$  propagator  $G_\Delta^{res}$  of Eq. (16) entering the isobaric current, contains imaginary parts. At low photon energies, where the damping effects of the  $\Delta$  propagator can only play a marginal role, one expects a plane wave calculation to produce  $P_y^p=0$ . This fundamental property can be exploited to check the numerical accuracy of the calculations. It speaks in favour of the calculations that the plane wave result at  $E_\gamma=100$  MeV does indeed obey this criterion for the full range of proton emission angles. At  $E_\gamma=100$  MeV, the polarization is thus fully determined by the FSI mechanisms. In the resonance region, the occurrence of the  $\Delta$  width would make a plane wave calculation already produce a  $P_y^p \neq 0$ . The  $P_y^p$  is then a measure for the medium-dependent damping mechanism of intermediate  $\Delta$  creation and the FSI effects. This is confirmed by the results in the right panel of Fig. 6, where neither of the two mechanisms is observed to be dominant.

Now we address the question in how far  $(\gamma, pp)$  polarization observables could be helpful in discriminating between the different model predictions for the ground-state correlation effects. Within the context of the present model this amounts to investigating the sensitivity to the different choices for the central correlation function (sometimes referred to as defect function). In order to minimize the contributions from the isobaric currents, we have considered quasi-deuteron kinematics and photon energies on either side of the  $\Delta_{33}$  resonance : (a)  $E_\gamma=100$  MeV and (b)  $E_\gamma=400$  MeV. Referring to Eq. (13) the effect of the ground-state correlations, which primarily comes through the magnetization current, is predicted to have a  $q_\gamma^2$  dependence, which make the SRC effects more likely to manifest themselves at higher photon energies. The left panel of Fig. 7, which refers to  $E_\gamma=100$  MeV, illustrates that even at lower photon energies the ground-state correlation effects do not overshoot the (suppressed) contribution from isobaric currents and exception made for the hard core correlation function of Ref. [47] (dot-dashed line) which is generally considered not to be very realistic. As a matter of fact, it is obvious from Fig. 7 that dedicated  $(\gamma, pp)$  experiments could unambiguously settle the unrealistic character of hard-core correlation functions. Remark that there are relatively little uncertainties regarding the  $\Delta$  current operator at low photon energies as the static limit for the isobaric current operator would be fully justified. Using realistic soft-core correlation functions, the ground-state correlation effects are relatively more visible in the differential cross section and proton polarization than in the photon asymmetry. At  $E_\gamma=400$  MeV the strength from the isobaric currents remains sizeable and the effect of the Jastrow correlations on the observables is of the same size than for  $E_\gamma=100$  MeV. The results of Fig. 7 illustrate that the mere fact of having the photon absorbed on a  ${}^1S_0$  diproton pair does not guarantee that the reaction process is dominated by ground-state correlations.

## B. $^{16}\text{O}(\gamma, NN)$ in coplanar and symmetrical kinematics

Coplanar and symmetrical kinematics refer to a specific situation for which the following kinematical conditions are obeyed : ( $|\vec{k}_a| = |\vec{k}_b| \equiv k$ ,  $\theta_a = \theta_b = \theta$ ,  $\phi_a = 0^\circ$ ,  $\phi_b = 180^\circ$ ). For each nucleon emission angle  $\theta$  and photonenergy, energy-momentum conservation will provide a unique solution for the momentum  $k$ . In the considered kinematics the c.m. momentum  $P$  varies rapidly with the polar angle  $\theta_a$  and within the factorized model of Subsect. III A we have  $|\vec{k}_+| = |\vec{k}_-| = \sqrt{k^2 \sin^2 \theta + q^2/4}$ . So, in many respects coplanar and symmetrical kinematics is complementary to QD kinematics. Whereas QD kinematics would rather be used to compare the relative motion of bound pairs with the deuteron, coplanar and symmetrical kinematics is intrinsically meant to explore the fact that in the medium nucleon pairs are characterized by c.m. degrees of freedom besides their relative motion. The strong dependence of the cross sections on the pair function  $F(P)$ , makes the absolute magnitude of the cross sections to vary dramatically as a function of the escaping nucleon angle in coplanar and symmetrical kinematics.

Within the factorized  $(\gamma, pp)$  model of Subsection III A, the major contribution from the central correlations to the cross section, which comes from a coupling of the photon field to the one-body magnetization current, is exactly zero for  $|\vec{k}_+| = |\vec{k}_-|$ . Accordingly, an abstraction made of the (small) contribution from the convection current, both the  $W_T$  and  $W_{TT}$  structure functions from Eq. (13) are predicted to be dominated by the isobaric current when facing coplanar and symmetrical kinematics.

Figure 8 displays the calculated  $^{16}\text{O}(\gamma, pp)$  and  $^{16}\text{O}(\gamma, pn)$  cross sections and photon asymmetries versus the proton emission angle and photon energy. We have considered a  $(1p_{1/2})^{-2}$  configuration for the residual A-2 nucleus, so that only  $J_R=0^+$  can contribute for the  $pp$  case, whereas the  $pn$  channel can feed two angular momenta states, namely  $J_R=0^+$  and  $1^+$ . For both channels and all emission angles considered a clear resonance at  $E_\gamma \approx 260$  MeV is observed for the cross section. The resonance is not very visible in the asymmetry. The  $pn$  channel is characterized by a wider photon energy and emission angle dependence than the  $pp$  breakup channel. In both cases, however, the pair function  $F(P)$  makes the strength to reside in these parts of the phase space for which the missing momentum  $P$  is small. At a fixed photon energy, the peak in the differential cross sections, which corresponds with the situation that the missing momentum is approximately zero, is localized at proton emission angles around 60-70 degrees in the lab frame. Remark that  $\theta_p \approx 70^\circ$  corresponds with zero missing momentum and the maximum of the cross section for the low end of the photon energies considered here. At higher photon energies ( $E_\gamma \geq 300$  MeV) the peak does gradually shift to 60 degrees in the lab frame. The  $P = 0$  situation in coplanar and symmetrical kinematics obeys also the QD conditions.

From the right panel of Fig. 8 it becomes clear that the  $(\gamma, pn)$  asymmetry is characterized by rather strong variations in both the photon energy and emission angle dependence. The smallest values are reached for the low photon energies. With increasing  $E_\gamma$  the isobaric currents gain in relative importance and as was already observed for the  $(\gamma, pn)$  results of Fig. 5 they tend to increase the asymmetry relative to the values that one would get including solely the meson-exchange contributions. The attention is drawn to the fact that the  $(\gamma, pp)$  results of the left panel in Fig. 8 represent a rather unique case in the sense that the selected  $(1p_{1/2})^{-2}$  final state can only feed the  $J_R=0^+$  state which gets its dominant contribution through  $(^1S_0, \Lambda=0)$  photoabsorption. An exception made for the lower photon energies, the proton-proton asymmetry is close to -1 for the full range of  $(E_\gamma, \theta_p)$  covered in Fig. 8. We remind that the asymmetry would be exactly -1 within the factorized model of Subsect. III A. This is another indication for the predictive power of the factorized model when  $^1S_0$  absorption is the dominant configuration. Our findings also confirm the calculations of Ref. [12], where it was pointed out that even after including the c.m. motion of the pair, simple  $^1S_0$  diproton breakup produces  $^3\text{He}(\vec{\gamma}, pp)$  asymmetries that are large and negative.

With the aim of studying in greater detail the impact of the different relative angular momentum states on the  $(\vec{\gamma}, pp)$  asymmetries we display model predictions for a  $((1p_{3/2})^{-2}; J_R = 0^+, 2^+)$  and a  $((1p_{3/2})^{-1}(1p_{1/2})^{-1}; J_R = 1^+)$  final state in Fig. 9. In comparison with the  $((1p_{1/2})^{-2}; J_R = 0^+)$  situation, the considered shell-model configurations are not as selective as far as the different contributing relative angular momentum states is concerned. Indeed, the  $(1p_{3/2})^{-2}$  configuration can be excited in proton-proton knockout through  $S$ ,  $P$  and  $D$  absorption. The  $((1p_{3/2})^{-1}(1p_{1/2})^{-1}; J_R = 1^+)$  configuration is unique in that  $S$ -wave absorption is excluded and only relative  $P$  waves would contribute in a Harmonic Oscillator model [7]. From the right panel of Fig. 9 it becomes clear that this produces a doubly-bumped structure in the  $\theta_p$  dependence with a minimum around  $P = 0$ . At the same time, the asymmetry is positive in most of the covered  $(E_\gamma, \theta_p)$  region. The left panel of Fig. 9 shows features that turn out to be a hybrid mixture of characteristics related to  $S$  and  $P$  wave absorption. The  $P$  wave admixture makes the asymmetry to be substantially smaller than what was obtained in the left panel of Fig. 8 where the  $S$  wave dominates. Rather strong variations of  $\Sigma$  in  $E_\gamma$  and  $\theta_p$  are observed and there is very little resemblance with a flat structure wiggling slightly above the  $\Sigma=-1$  plane as was noticed for the  $(\gamma, pp)$  results in Fig. 8. So, rather than FSI effects or Fermi motion it turns out that photoabsorption on relative  $P$  diprotons has a very large impact on the  $(\vec{\gamma}, pp)$  asymmetries. The present results seem to suggest that an admixture of  $P$ -wave absorption might also help in interpreting the measured

${}^3\text{He}(\vec{\gamma}, pp)$  asymmetries (Ref. [10]) which were shown to be incompatible with  ${}^1S_0$  photoabsorption in Ref. [12].

In an attempt to study the photonenergy dependence of the  $(\gamma, pp)$  variables more profoundly and estimate the effect of the ground-state correlations, we display in Fig. 10 some cuts along fixed values of the opening angle in the three-dimensional plot of Fig. 8. The opening angles are chosen to lie in that part of the phase space where the cross sections are reasonably large. Four values of the opening angles have been considered. The sensitivity of the cross sections to the ground-state correlations is found to be relatively small. So is the effect on the asymmetry for most of the phase space covered. However, the spike observed at  $\theta_p=90^\circ$  and lower photon energies (see also Fig. 8) has to be fully ascribed to the ground-state correlations. It is maybe worth stressing that  $\theta_p=90^\circ$  corresponds with the situation that the largest values of the relative pair momentum are reached in coplanar and symmetrical kinematics. The effect of the short-range effects on the proton polarization is large. This might however be very characteristic for the chosen shell-model configuration in the final state. Indeed, the proton polarization turns out to be zero when considering only the isobaric contribution and a  $0^+$  final state.

The corresponding  $(\gamma, pn)$  results for the proton-proton results in Fig. 10 are contained in Fig. 11. For all nucleon emission angles considered, a wide  $\Delta$  resonant structure is visible in the cross section. Surprisingly, the resonant behaviour is not pronounced for the polarization observables. This confirms the conclusion that the asymmetry is extremely sensitive to the interference terms between the different contributing two-body operators. Remark that the predicted effect of central ground-state correlations on the  $(\gamma, pn)$  observables is marginal.

## V. CONCLUSIONS AND PROSPECTS

In this paper we have explored the possibilities of using polarized photon beams and outgoing nucleon polarimetry to learn more about the dynamics of bound nucleon pairs with the aid of  $(\gamma, pp)$  and  $(\gamma, pn)$  reactions. As it is often the case, the asymmetry was shown to be less dependent on the outgoing nucleon distortions than the corresponding differential cross sections. The effect of the outgoing nucleon distortions on the polarization, however, is rather large. The  $P_y^p$  was further shown to be a sensitive observable to investigate the mechanisms related to the short lifetime of the  $\Delta$  resonance in the medium. Indeed, the latter reflect themselves in imaginary parts entering the  $\Delta$  selfenergy and produce sizeable contributions to the outgoing nucleon polarization.

It was pointed out that by studying the differential cross sections for excitation of the  $A-2$  fragment in a state with particular angular momentum  $J_R$  one can deduce information about the nature of the initial pair wave function. This does not imply, however, that the experiments would have to resolve each residual state. Observables for different shell combinations, which would typically feed the residual system in a certain range of missing energies, would already be very instructive to learn about the different possible pair combinations. We have shown that the observables are characterized by a selective sensitivity to mechanisms that go beyond photoabsorption on a  ${}^1S_0$  proton-proton and  ${}^3S_1$  proton-neutron pair. This was found to be already the case in so-called quasi-deuteron kinematics where the missing momentum is constrained to be zero, so that the influence of the pair c.m. motion is minimized and “deuteron-like” conditions are created. In this type of kinematics, the major deviations from S-wave absorption are visible in the angular cross sections. The polarization observables seem to be far less affected. The fact that S-wave absorption plays a predominant role does not guarantee, however, that the  $(\gamma, pn)$  asymmetries exhibit deuteron-like properties in quasi-deuteron kinematics. In the  $\Delta$  resonance region a strong similarity between the  $d(\vec{\gamma}, pn)$  and the  ${}^{12}\text{C}(\vec{\gamma}, pn)$  asymmetries is observed. The situation changes for the lower photon energies where the  ${}^{12}\text{C}$  predictions deviate substantially from the measured deuteron asymmetries. For all these reasons, we deem that the exclusive  $(\gamma, NN)$  channel is an ideal probe to study the limitations of the QD approach and to reach a better level in our understanding of the dynamics of proton-neutron pairs in the medium relative to the deuteron.

Within the factorized model, a general behaviour for the  $A(\vec{\gamma}, pp)$  asymmetries is predicted in that they would be exactly -1 as long as one is dealing with  ${}^1S_0$  absorption in coplanar kinematics and the dominant role of the isobar current is guaranteed. Neither FSI effects, nor a more sophisticated treatment of the pair relative  $S$  wave function seem to change this very much. The slightest admixture of mechanisms going beyond  ${}^1S_0$  absorption are noticed to induce major changes to the asymmetry. Whereas  $\Sigma \approx -1$  for  ${}^1S_0$  photoabsorption, the calculations predict a completely different behaviour as soon as relative  $P, D, \dots$  start playing a role. The extent to which mechanisms beyond  $S$  wave absorption play a role is very much dependent on the kinematics and the nuclear structure of the  $A-2$  fragment. The sensitivity of the  $(\gamma, pp)$  asymmetries to ground-state correlations was shown not to be very large and was considerably smaller than the effects on the angular cross sections and outgoing nucleon polarizations. Such a behaviour could already be inferred from the expressions derived within the context of the factorized model. All this, however, is illustrating the usefulness of having simplified models for predicting the major trends and sensitivities in the different observables.

It would be of interest to see to which degree the deviations from QD-like absorption and deuteron-like behaviour

can be experimentally confirmed. In any case, high or moderate resolution data in the low-energy part of the missing energy spectrum would provide invaluable information to test whether the dynamics of the pairs in the medium complies with mean-field like behaviour or whether there are important deviations in (some of) the relative wave function combinations. In order to minimize the uncertainties regarding the final state interaction polarization observables, and in particular the photon asymmetries, will be of very great help in these studies.

### ACKNOWLEDGMENT

This work was supported by the Fund for Scientific Research - Flanders (FWO) and in part by the NATO through the research grant CRG970268. One of us (J.R.) thanks the Institute for Nuclear Theory at the University of Washington for partial support during the completion of this work.

- [1] K. Gottfried, Nucl. Phys. **5**, 557 (1958).
- [2] S. Homma, M. Kanazawa, M. Koike, Y. Murata, H. Okuno, F. Soga, N. Yoshikawa and A. Sasaki, Phys. Rev. Lett. **52**, 2026 (1984).
- [3] S.N. Dancer *et al.*, Phys. Rev. Lett. **61**, 1170 (1988).
- [4] P.D. Harty *et al.*, Phys. Lett. **B380**, 247 (1996).
- [5] P. Grabmayr *et al.*, Phys. Lett. **B370**, 17 (1996).
- [6] K.I. Blomqvist *et al.*, submitted for publication.
- [7] C.J.G. Onderwater *et al.*, Phys. Rev. Lett. **78**, 4893 (1997).
- [8] M. Kanazawa *et al.*, Phys. Rev. **C35**, 1828 (1987).
- [9] J. Arends *et al.*, Z. Phys. **A298**, 103 (1980).
- [10] D.J. Tedeshi *et al.*, Phys. Rev. Lett. **73**, 408 (1994).
- [11] H. Baghaei *et al.*, Proceedings of the Second Workshop on Electromagnetically Induced Two-Nucleon Emission (Gent, May 17-20, 1995), Eds. J. Ryckebusch and M. Waroquier, (University of Gent publication, 1995), 195 and R. Lindgren *et al.*, submitted for publication.
- [12] A.M. Sandorfi and W. Leidemann, Phys. Rev. C **53**, 1506 (1996).
- [13] P. Wilhelm, J.A. Niskanen and H. Arenhövel, Nucl. Phys. **A597**, 613 (1996).
- [14] R.C. Carrasco, M.J. Vicente Vacas and E. Oset, Nucl. Phys. **A570**, 701 (1994).
- [15] G. Cross *et al.*, Nucl. Phys. **A593**, 463 (1995).
- [16] N. Kolb *et al.*, Proceedings of the Second Workshop on Electromagnetically Induced Two-Nucleon Emission (Gent, May 17-20, 1995), Eds. J. Ryckebusch and M. Waroquier, (University of Gent publication, 1995), 179.
- [17] Th. Lamparter *et al.*, Z. Phys. A **355**, 1 (1996).
- [18] C. Giusti and F.D. Pacati, Nucl. Phys. **A585**, 618 (1995).
- [19] J. Ryckebusch, M. Vanderhaeghen, L. Macheuil and M. Waroquier, Nucl. Phys. **A568**, 828 (1994).
- [20] S. Boffi, C. Giusti, F.D. Pacati and M. Radici, Nucl. Phys. **A564**, 473 (1993).
- [21] C. Giusti and F.D. Pacati, Nucl. Phys. **A615**, 673 (1997).
- [22] J. Ryckebusch, V. Van der Sluys, K. Heyde, H. Holvoet, W. Van Nespén, M. Waroquier and M. Vanderhaeghen, Nucl. Phys. A (1997), in print.
- [23] M. Wakamatsu and K. Matsumoto, Nucl. Phys. **A392**, 323 (1982).
- [24] M.-Th. Hütt, A.I. Milstein and M. Schumacher, Nucl. Phys. **A618**, 483 (1997).
- [25] T. Ericson and W. Weise, *in* Pions and Nuclei (Oxford University Press, New York, 1988).
- [26] M. Vanderhaeghen, K. Heyde, J. Ryckebusch and M. Waroquier, Nucl. Phys. **A595**, 219 (1995).
- [27] I.S. Towner, Phys. Rep. **155**, 263 (1987).
- [28] L. Boato and M.M. Giannini, J. Phys. G. **15**, 1605 (1989).
- [29] J. Ryckebusch, L. Macheuil, M. Vanderhaeghen and M. Waroquier, Phys. Lett. **B291**, 213 (1992).
- [30] J. Ryckebusch, Phys. Lett. **B383**, 1 (1996).
- [31] M. Vanderhaeghen, L. Macheuil, J. Ryckebusch and M. Waroquier, Nucl. Phys. **A580**, 551 (1994).
- [32] E. Oset and L.L. Salcedo, Nucl. Phys. **A468**, 631 (1987).
- [33] M. Waroquier, J. Ryckebusch, J. Moreau, K. Heyde, N. Blasi, S.Y. van der Werf and G. Wenes, Phys. Rept. **148**, 249 (1987).
- [34] V. Van der Sluys, K. Heyde, J. Ryckebusch and M. Waroquier, Phys. Rev. C **55**, 1982 (1997).
- [35] I.J.D. MacGregor *et al.*, submitted for publication.

- [36] G. Garino *et al.*, Phys. Rev. C **45**, 780 (1992).  
V.R. Pandharipande and Steven C. Pieper, Phys. Rev. C **45**, 791 (1992).
- [37] K. Heyde, The Nuclear Shell-Model (Springer Verlag, Berlin Heidelberg, 1994).
- [38] L. Isaksson, Ph.D. thesis, Department of Physics, University of Lund (1996).
- [39] H. Arenhövel and M. Sanzone, *Photodisintegration of the deuteron, in Few Body Systems -Supplementum 3*, (Springer Verlag, Wien, 1991).
- [40] F. Ritz, H. Arenhövel and T. Wilbois, University of Mainz preprint MKPH-T-97-19, nucl-th/9707045.
- [41] M.I. Levchuk, Few-Body Systems **19**, 77 (1995).
- [42] C.C. Gearhart, PhD thesis, University of Washington (1994) unpublished, and W. Dickhoff, private communication.
- [43] G. Blanpied *et al.*, Phys. Rev. C **52**, R455 (1995) and LEGS Data Release L1-3.0 available from <http://www.legs.bnl.gov/~legs/>.
- [44] V.G. Gorbenko, Yu.V. Zhebrovskij, L.Ya. Kolesnikov, A.L. Rubashkin and P.V. Sorokin, Nucl. Phys. **A381**, 330 (1982).
- [45] V.B. Ganenko *et al.*, Z. Phys. A. **341**, 205 (1992).
- [46] I. Arias de Saavedra *et al.*, Nucl. Phys. **A605**, 354 (1996).
- [47] J.W. Clark, Lecture Notes in Physics **138**, Eds. R. Guardiola and J. Ros (Springer Verlag, Berlin, 1981) p 184.

TABLE I. Possible configurations for proton-proton knockout from the s- and p-shell combinations. The  $\Lambda$  ( $l$ ) denotes the c.m. (relative) angular momentum of the pair. The  $J_{pair}^\pi$  is the total angular momentum of the pair (including relative and c.m. motion). The separation in c.m. and relative motion is done as if we are dealing with HO single-particle wave functions.

shell-model ( $n_h, l_h$ )( $n_{h'}, l_{h'}$ )	(L,S) $J_{pair}^\pi$	relative ( $n, l$ )	c.m. ( $N, \Lambda$ )	relative wave function $^{2S+1}l_J$ (T)
(1s) <sup>2</sup>	(0, 0)0 <sup>+</sup>	(1, 0)	(1, 0)	<sup>1</sup> S <sub>0</sub> (T=1)
(1s)(1p)	(1, 1)0 <sup>-</sup>	(1, 1)	(1, 0)	<sup>3</sup> P <sub>0</sub> (T=1)
	(1, 0)1 <sup>-</sup>	(1, 0)	(1, 1)	<sup>1</sup> S <sub>0</sub> (T=1)
	(1, 1)1 <sup>-</sup>	(1, 1)	(1, 0)	<sup>3</sup> P <sub>1</sub> (T=1)
	(1, 1)2 <sup>-</sup>	(1, 1)	(1, 0)	<sup>3</sup> P <sub>2</sub> (T=1)
(1p) <sup>2</sup>	(0, 0)0 <sup>+</sup>	(1, 0)	(2, 0)	<sup>1</sup> S <sub>0</sub> (T=1)
	(0, 0)0 <sup>+</sup>	(2, 0)	(1, 0)	<sup>1</sup> S <sub>0</sub> (T=1)
	(1, 1)0 <sup>+</sup>	(1, 1)	(1, 1)	<sup>3</sup> P <sub>1</sub> (T=1)
	(1, 1)1 <sup>+</sup>	(1, 1)	(1, 1)	<sup>3</sup> P <sub>0</sub> , <sup>3</sup> P <sub>1</sub> , <sup>3</sup> P <sub>2</sub> (T=1)
	(1, 1)2 <sup>+</sup>	(1, 1)	(1, 1)	<sup>3</sup> P <sub>1</sub> , <sup>3</sup> P <sub>2</sub> (T=1)
	(2, 0)2 <sup>+</sup>	(1, 0)	(1, 2)	<sup>1</sup> S <sub>0</sub> (T=1)
	(2, 0)2 <sup>+</sup>	(1, 2)	(1, 0)	<sup>1</sup> D <sub>2</sub> (T=1)

TABLE II. Possible configurations for proton-neutron knockout from the s- and p-shell combinations. The  $\Lambda$  ( $l$ ) denotes the c.m. (relative) angular momentum of the pair. The  $J_{pair}^\pi$  is the total angular momentum of the pair (including relative and c.m. motion). The separation in c.m. and relative motion is done as if we are dealing with HO single-particle wave functions.

shell-model ( $n_h, l_h$ )( $n_{h'}, l_{h'}$ )	(L,S) $J_{pair}^\pi$	relative ( $n, l$ )	c.m. ( $N, \Lambda$ )	relative wave function $^{2S+1}l_J$ (T)
(1s) <sup>2</sup>	(0, 0)0 <sup>+</sup>	(1, 0)	(1, 0)	<sup>1</sup> S <sub>0</sub> (T=1)
	(0, 1)1 <sup>+</sup>	(1, 0)	(1, 0)	<sup>3</sup> S <sub>1</sub> (T=0)
(1s)(1p)	(1, 1)0 <sup>-</sup>	(1, 0)	(1, 1)	<sup>3</sup> S <sub>1</sub> (T=0)
	(1, 1)0 <sup>-</sup>	(1, 1)	(1, 0)	<sup>3</sup> P <sub>0</sub> (T=1)
	(1, 0)1 <sup>-</sup>	(1, 1)	(1, 0)	<sup>1</sup> P <sub>1</sub> (T=0)
	(1, 0)1 <sup>-</sup>	(1, 0)	(1, 1)	<sup>1</sup> S <sub>0</sub> (T=1)
	(1, 1)1 <sup>-</sup>	(1, 0)	(1, 1)	<sup>3</sup> S <sub>1</sub> (T=0)
	(1, 1)1 <sup>-</sup>	(1, 1)	(1, 0)	<sup>3</sup> P <sub>1</sub> (T=1)
	(1, 1)2 <sup>-</sup>	(1, 0)	(1, 1)	<sup>3</sup> S <sub>1</sub> (T=0)
(1p) <sup>2</sup>	(1, 1)2 <sup>-</sup>	(1, 1)	(1, 0)	<sup>3</sup> P <sub>2</sub> (T=1)
	(0, 0)0 <sup>+</sup>	(2, 0)	(1, 0)	<sup>1</sup> S <sub>0</sub> (T=1)
	(0, 0)0 <sup>+</sup>	(1, 0)	(2, 0)	<sup>1</sup> S <sub>0</sub> (T=1)
	(1, 1)0 <sup>+</sup>	(1, 1)	(1, 1)	<sup>3</sup> P <sub>1</sub> (T=1)
	(0, 1)1 <sup>+</sup>	(2, 0)	(1, 0)	<sup>3</sup> S <sub>1</sub> (T=0)
	(0, 1)1 <sup>+</sup>	(1, 0)	(2, 0)	<sup>3</sup> S <sub>1</sub> (T=0)
	(1, 1)1 <sup>+</sup>	(1, 1)	(1, 1)	<sup>3</sup> P <sub>0</sub> , <sup>3</sup> P <sub>1</sub> , <sup>3</sup> P <sub>2</sub> (T=1)
	(1, 0)1 <sup>+</sup>	(1, 1)	(1, 1)	<sup>1</sup> P <sub>1</sub> (T=0)
	(2, 1)1 <sup>+</sup>	(1, 0)	(1, 2)	<sup>3</sup> S <sub>1</sub> (T=0)
	(2, 1)1 <sup>+</sup>	(1, 2)	(1, 0)	<sup>3</sup> D <sub>1</sub> (T=0)
	(1, 1)2 <sup>+</sup>	(1, 1)	(1, 1)	<sup>3</sup> P <sub>1</sub> , <sup>3</sup> P <sub>2</sub> (T=1)
	(2, 0)2 <sup>+</sup>	(1, 0)	(1, 2)	<sup>1</sup> S <sub>0</sub> (T=1)
	(2, 0)2 <sup>+</sup>	(1, 2)	(1, 0)	<sup>1</sup> D <sub>2</sub> (T=1)
	(2, 1)2 <sup>+</sup>	(1, 0)	(1, 2)	<sup>3</sup> S <sub>1</sub> (T=0)
	(2, 1)2 <sup>+</sup>	(1, 2)	(1, 0)	<sup>3</sup> D <sub>2</sub> (T=0)
(2, 1)3 <sup>+</sup>	(1, 0)	(1, 2)	<sup>3</sup> S <sub>1</sub> (T=0)	
(2, 1)3 <sup>+</sup>	(1, 2)	(1, 0)	<sup>3</sup> D <sub>3</sub> (T=0)	

FIG. 1. Basic diagrams contributing to photopion production on the nucleon. The diagrams are drawn in a rather uncommon fashion so as to make the link with photoinduced  $2N$  knockout more clear (Fig. 2). (a) Kroll-Rudermann term ; (b) pion-pole term ; (c,f) direct and crossed nucleon Born terms ; (d,e) direct and crossed  $\Delta$  terms.

FIG. 2. The equivalent diagrams of Fig. 1 for two-nucleon knockout from finite nuclei in the spectator approximation. Each solid line shows a nucleon moving in a mean-field potential.

FIG. 3. Unpolarized differential cross section, photon asymmetry and proton polarization for the  $^{12}\text{C}(\gamma, pp)^{10}\text{Be}((1p_{3/2})^{-2})$  at  $E_\gamma=100, 200, 300$  and  $400$  MeV in QD kinematics. The separate contribution from  $J_R=0^+$  (dashed line) and  $J_R=2^+$  (dotted line) are shown. The solid line is the incoherent sum of both contributions. The curves are the result of an unfactorized calculation including outgoing nucleon distortions, isobaric currents and ground-state correlations. The latter are implemented with the central correlation function from Ref. [42].

FIG. 4. Unpolarized differential cross section, photon asymmetry and proton polarization for the  $^{12}\text{C}(\gamma, pn)^{10}\text{B}((1p_{3/2})^{-2})$  reaction at  $E_\gamma=100, 200, 300$  and  $400$  MeV in QD kinematics. The separate contribution from  $J_R=0^+$  (dashed line),  $J_R=1^+$  (dot-dashed line) and  $J_R=3^+$  (dotted line) are shown. The  $J_R=2^+$  component is small and has been omitted from the figure. The solid line is the incoherent sum of all  $J_R$  components. The curves are the result of an unfactorized calculation including outgoing nucleon distortions, pion exchange currents, isobaric currents and ground-state correlations. The latter are implemented with the central correlation function from Ref. [42]. The asymmetries are compared with  $d(\vec{\gamma}, p)n$  data from Refs. [43] (triangles) and [44] (squares). The proton polarization is compared with  $d(\gamma, \vec{p})n$  data from Ref. [45].

FIG. 5. Unpolarized differential cross section, photon asymmetry and proton polarization for the  $^{16}\text{O}(\gamma, pn)$  reaction for two types of p-shell configurations in QD kinematics and  $E_\gamma=150$  MeV. The dashed line is obtained when including only the seagull pion-exchange current. The dotted line is the calculated result when including both the seagull and pion-in-flight pion-exchange current. The solid line shows the full model calculation, including the two pion exchange and the  $\Delta_{33}$  currents. The dot-dashed line shows the equivalent result but now using plane waves for the outgoing particle wave functions.

FIG. 6. Differential cross section, asymmetry and polarization for the  $^{12}\text{C}(\gamma, pp)^{10}\text{Be}((1p_{3/2})^{-2})$  reaction at  $E_\gamma=100$  and  $300$  MeV in QD kinematics. The dotted curves are the predictions of the factorized model. The solid (dashed) line are the results of the unfactorized model using distorted (plane) outgoing nucleon waves. In all cases isobaric currents and ground-state correlations are included. The latter are implemented with the central correlation function from Ref. [42].

FIG. 7. The  $^{12}\text{C}(\gamma, pp)$  observables in QD kinematics for knockout from the p-shell. All curves are obtained in the unfactorized model and include outgoing nucleon distortions. The dashed line includes solely the isobaric currents. The other curves include also Jastrow correlations with different choices for the correlation function : Ref. [42] (solid), Ref. [46] (dotted) and Ref. [47] (dot-dashed).

FIG. 8. Photon energy and proton emission angle dependency of the  $^{16}\text{O}(\gamma, pp)(1p_{1/2})^{-2}$  and  $^{16}\text{O}(\gamma, pn)(1p_{1/2})^{-2}$  differential cross section and photon asymmetry in coplanar and symmetrical kinematics. The calculations include the outgoing nucleon distortions and all contributing meson-exchange and isobaric current diagrams. Ground-state correlations were implemented through the correlation function from Ref. [42].

FIG. 9. Photon energy and emission angle dependency of the  $^{16}\text{O}(\gamma, pp)^{14}\text{C}$  differential cross section and asymmetry in coplanar and symmetrical kinematics. Two different shell-model configurations are considered. The calculations include the outgoing nucleon distortions and all contributing isobaric current diagrams. Also the ground-state correlations were implemented using the correlation function from Ref. [42].

FIG. 10. Photon energy dependency of cross section, asymmetry and polarization for the  $^{16}\text{O}(\gamma, pp)^{14}\text{C}((1p_{1/2})^{-2}, J_R = 0^+)$  reaction in coplanar and symmetrical kinematics and different values for the opening angle  $\theta_p$ . The curves are the result of an unfactorized calculation including outgoing nucleon distortions. The dashed curves are the results when including solely isobaric currents. For the solid lines also the effect of ground-state correlations are included. The latter are implemented with the central correlation function from Ref. [42].

FIG. 11. Photon energy dependency of cross section, asymmetry and polarization for the  $^{16}\text{O}(\gamma, pn)^{14}\text{N}((1p_{1/2})^{-2})$  reaction in coplanar and symmetrical kinematics and different values for the opening angle  $\theta_p = \theta_n$ . The contributions from  $J_R = 0^+$  and  $1^+$  are incoherently added. The dashed curves are the result of an unfactorized calculation including outgoing nucleon distortions, meson exchange and isobaric currents. For the solid lines also the effect of ground-state correlations are included. The latter are implemented with the central correlation function from Ref. [42].



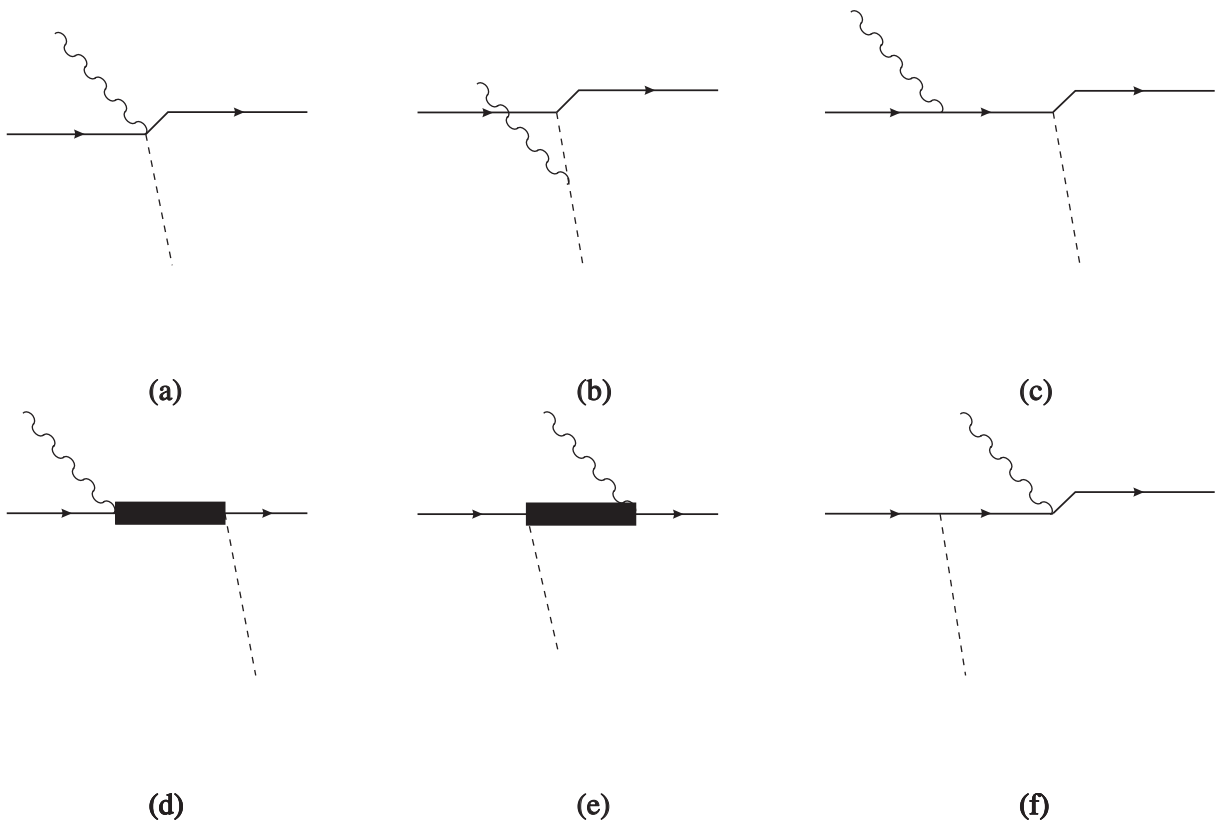


Figure 1

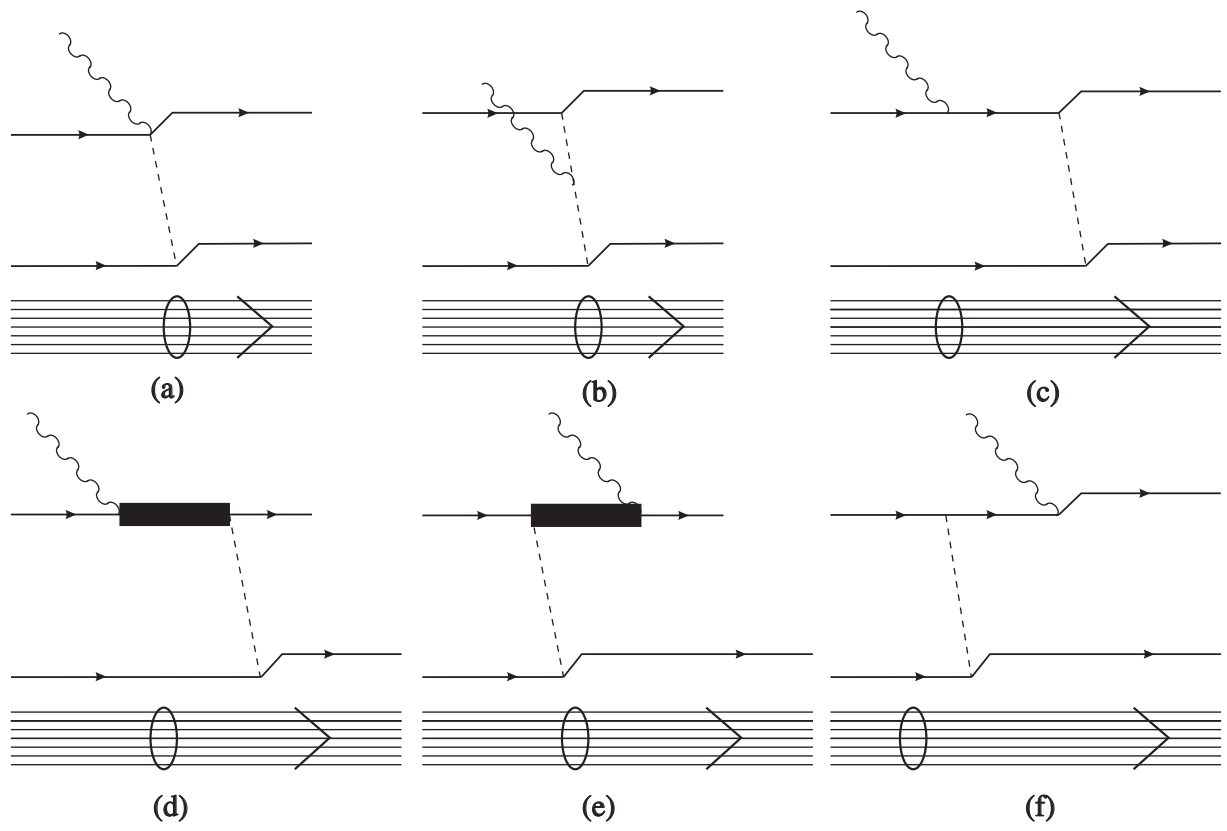


Figure 2

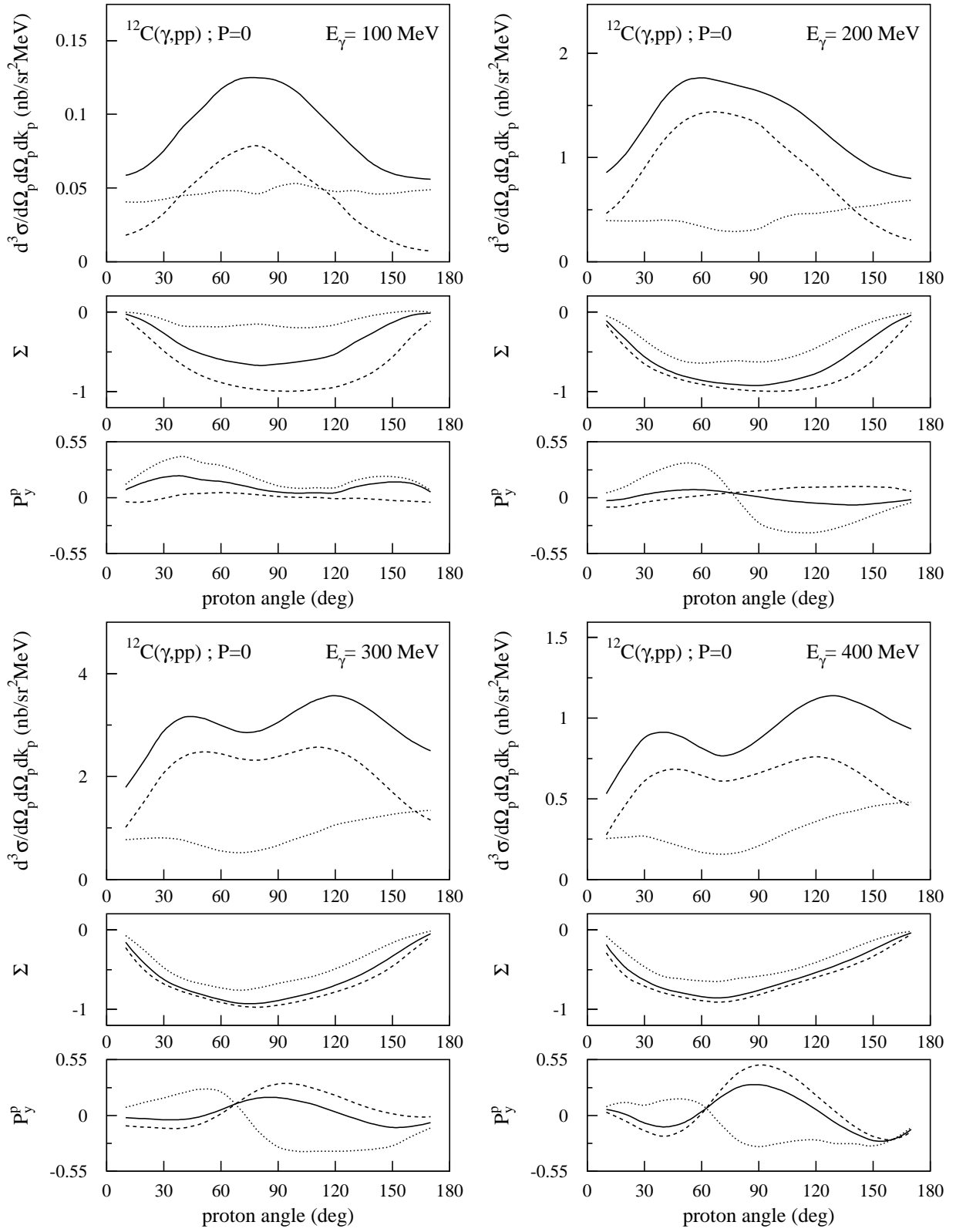


Figure 3

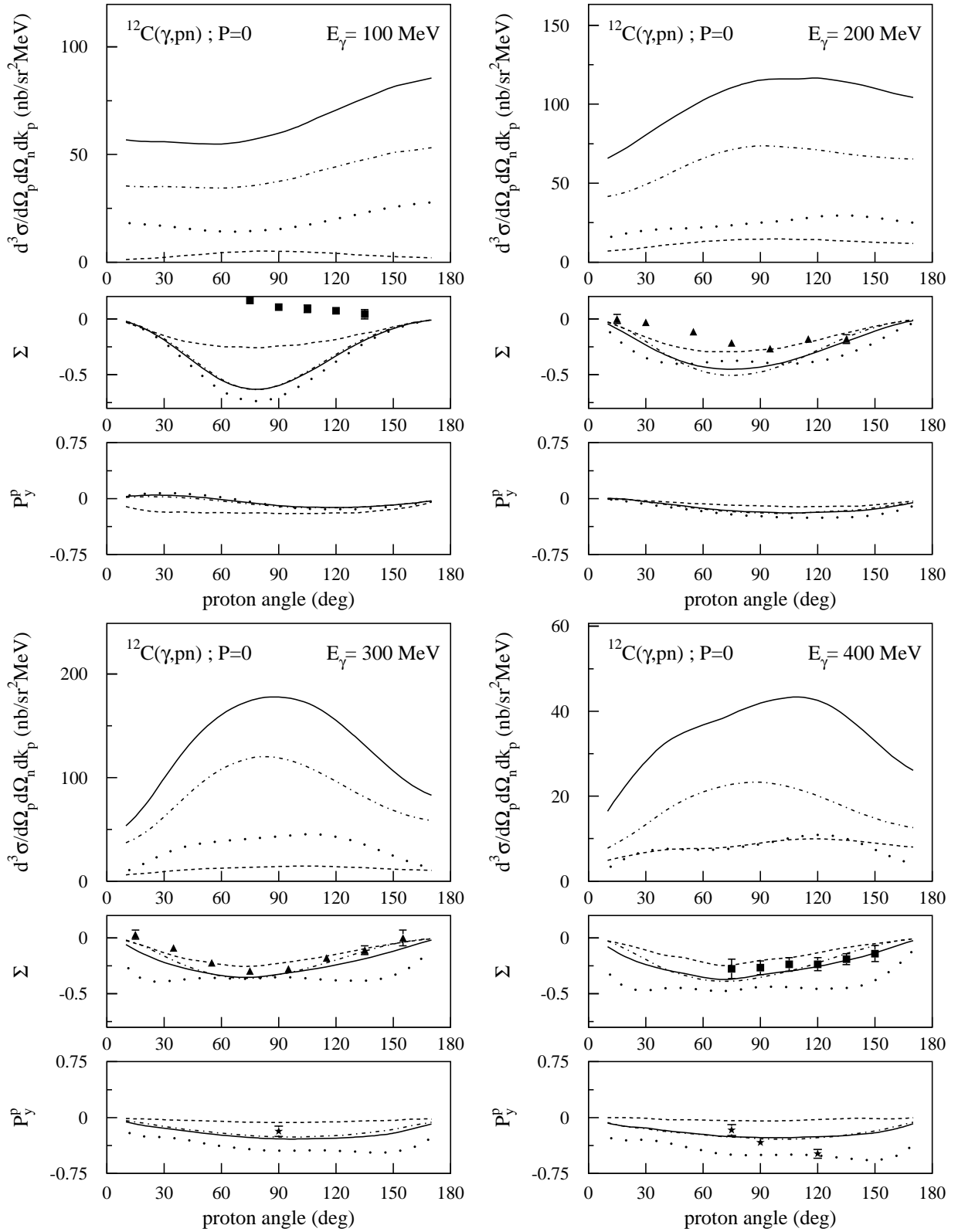


Figure 4

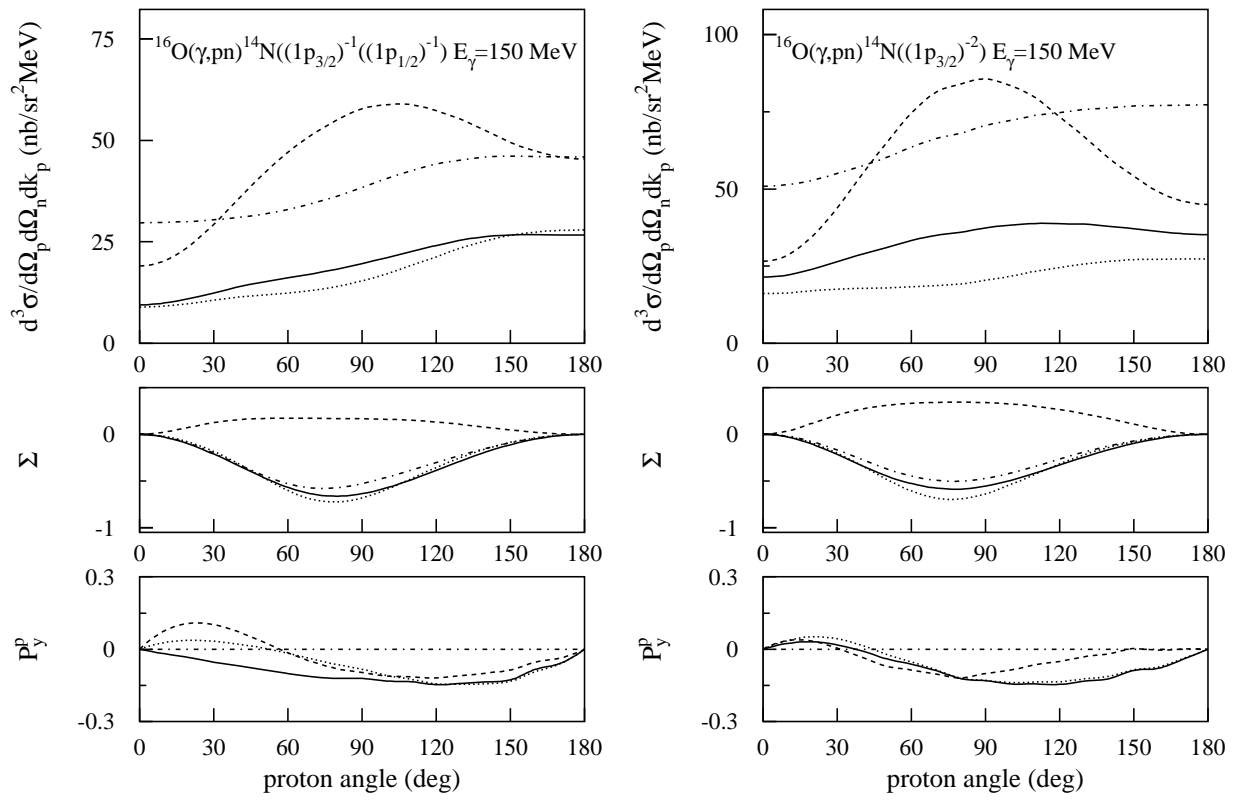


Figure 5

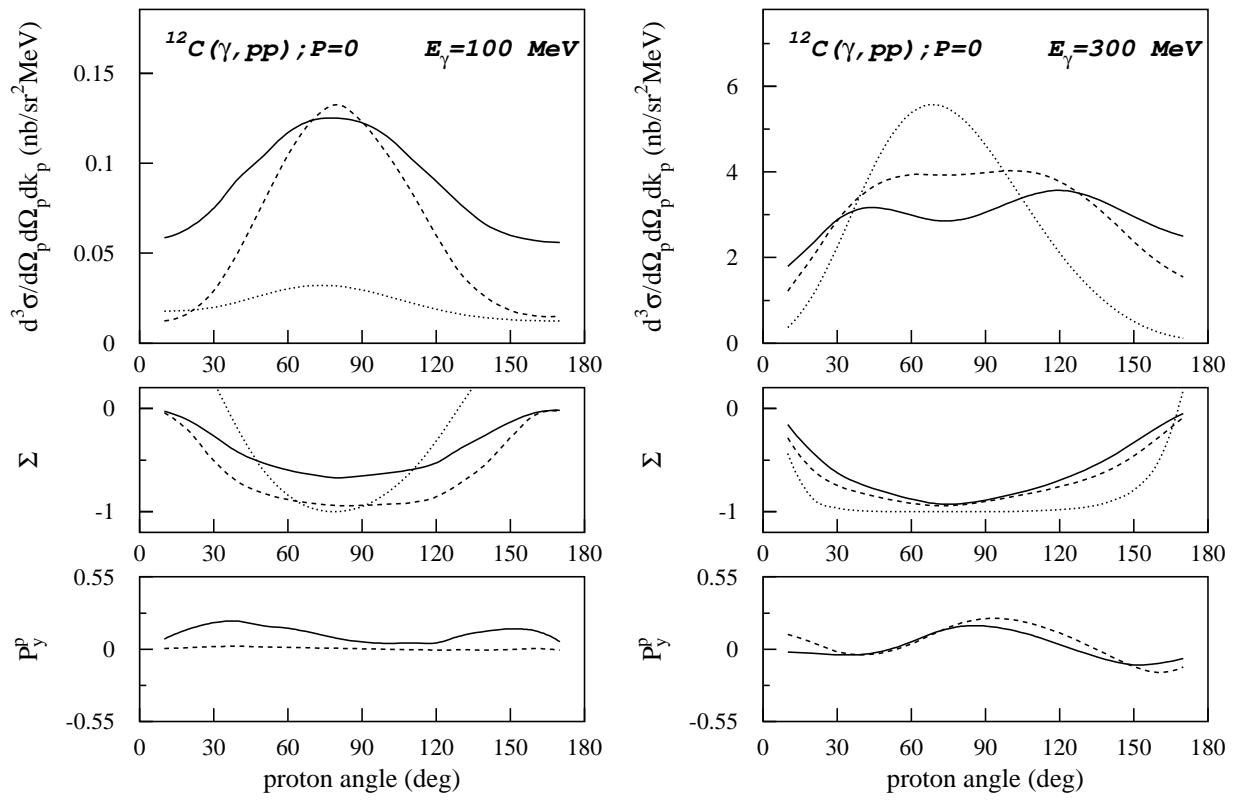


Figure 6

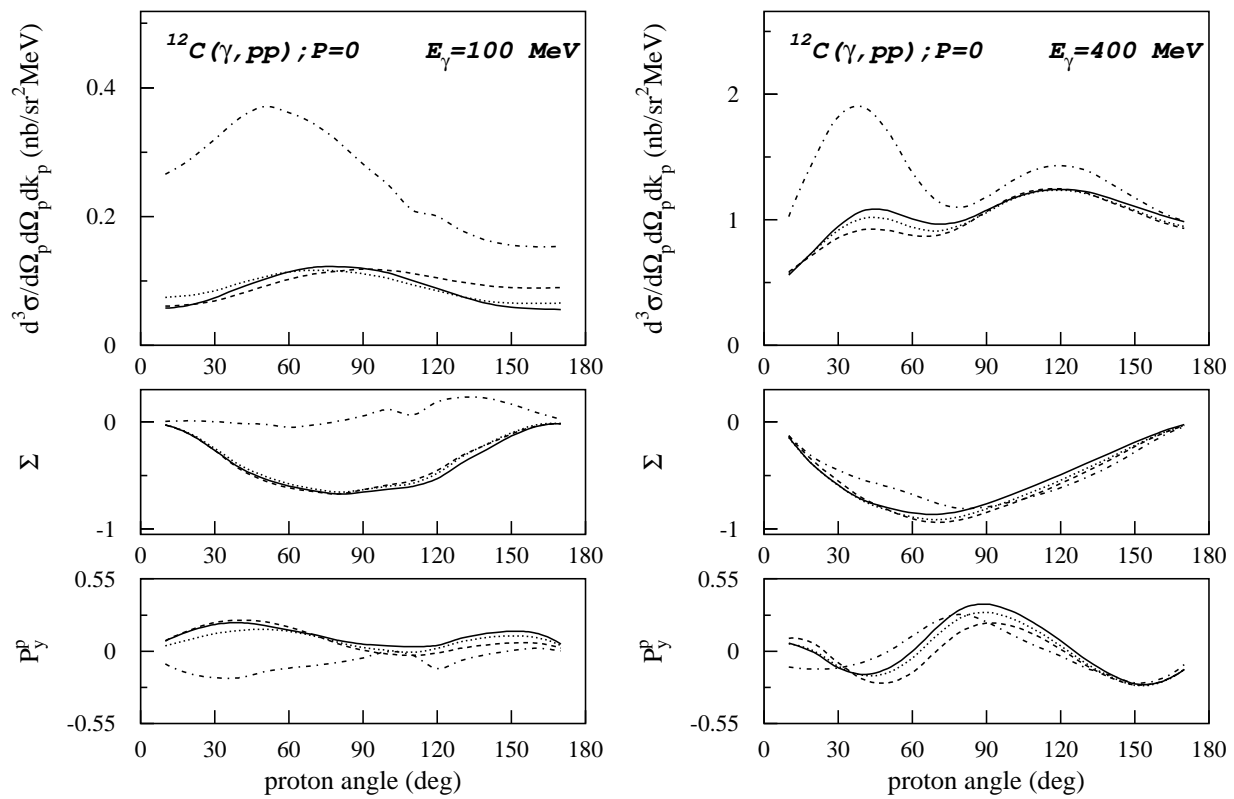


Figure 7

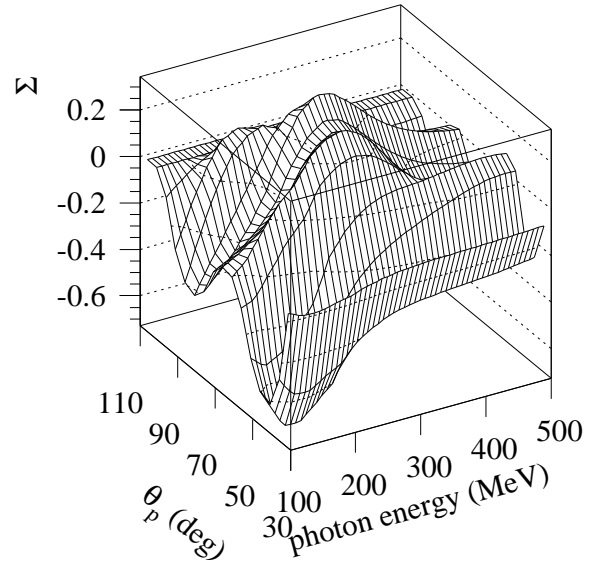
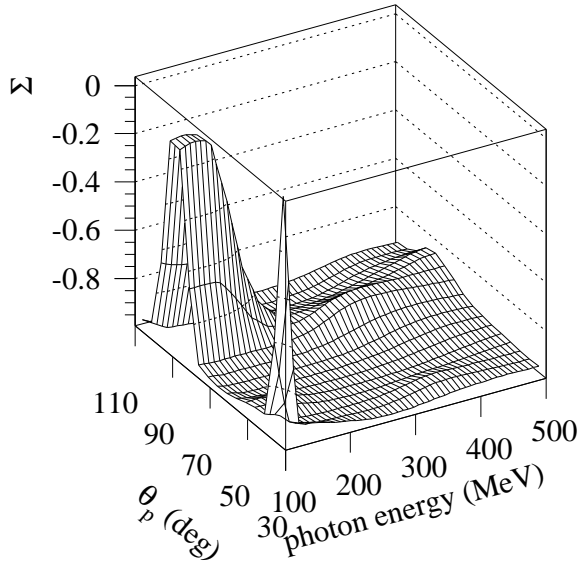
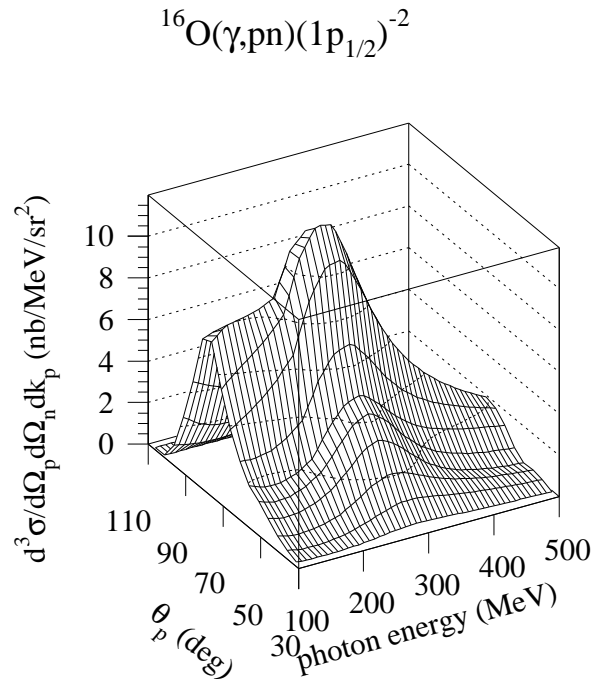
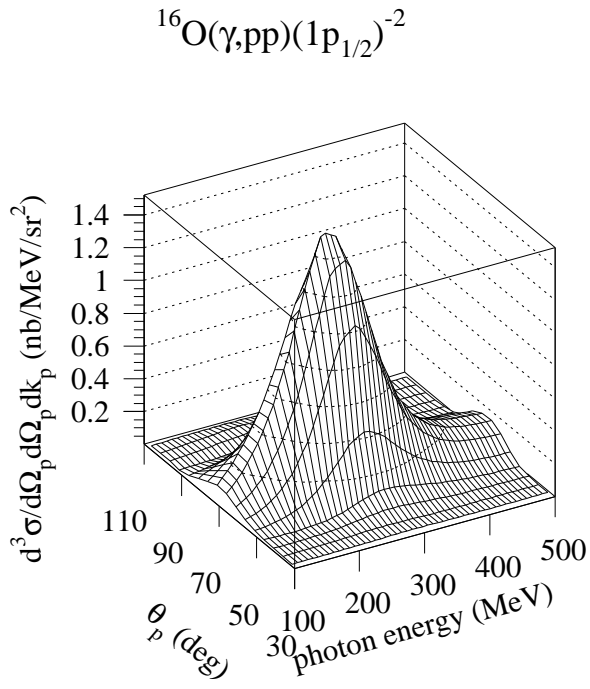


Figure 8



$$^{16}\text{O}(\gamma,pp)((1p_{3/2})^{-2}); J_R=0^+, 2^+$$

$$^{16}\text{O}(\gamma,pp)((1p_{3/2})^{-1}(1p_{1/2})^{-1}); J_R=1^+$$

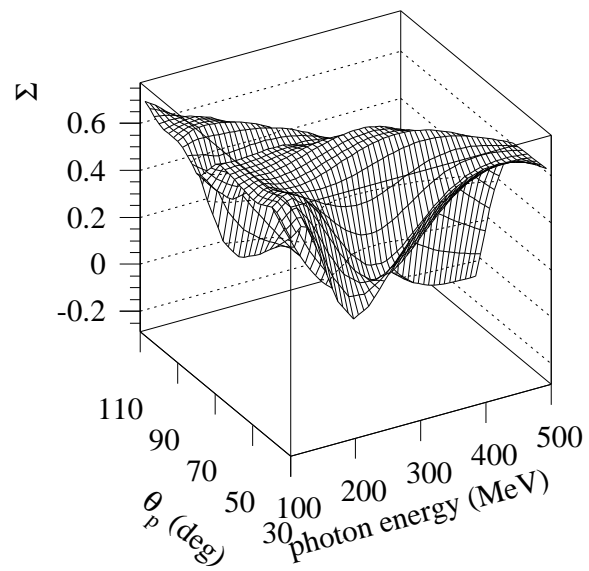
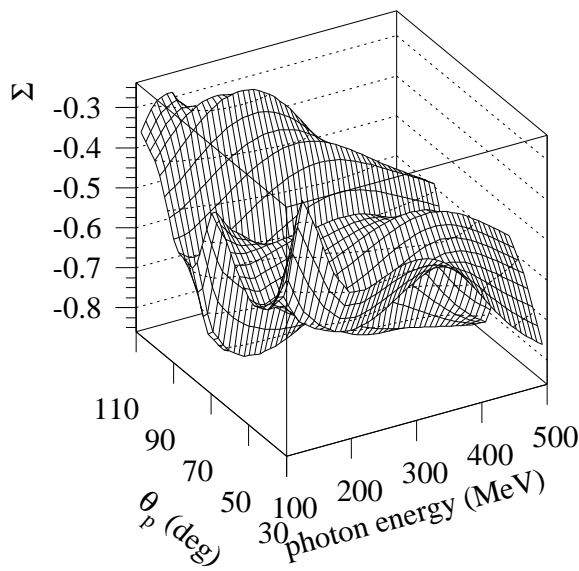
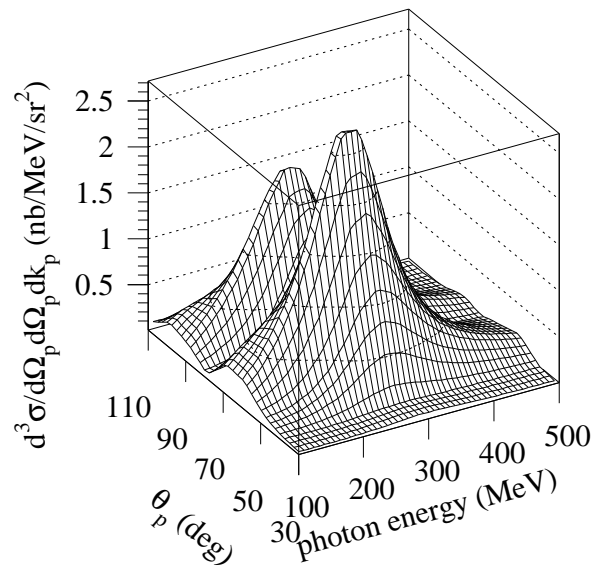
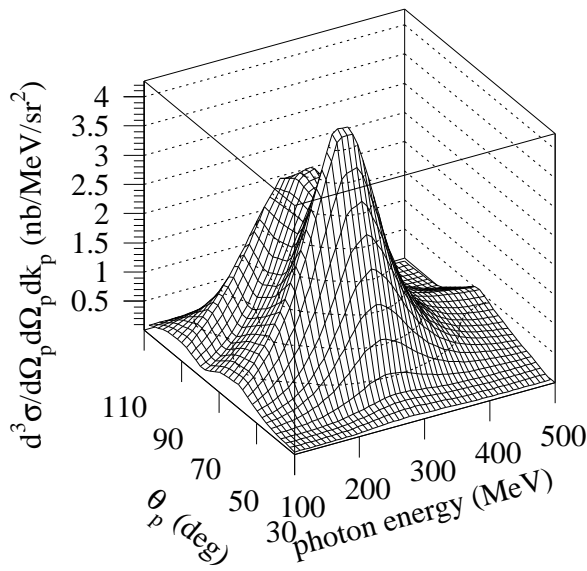


Figure 9

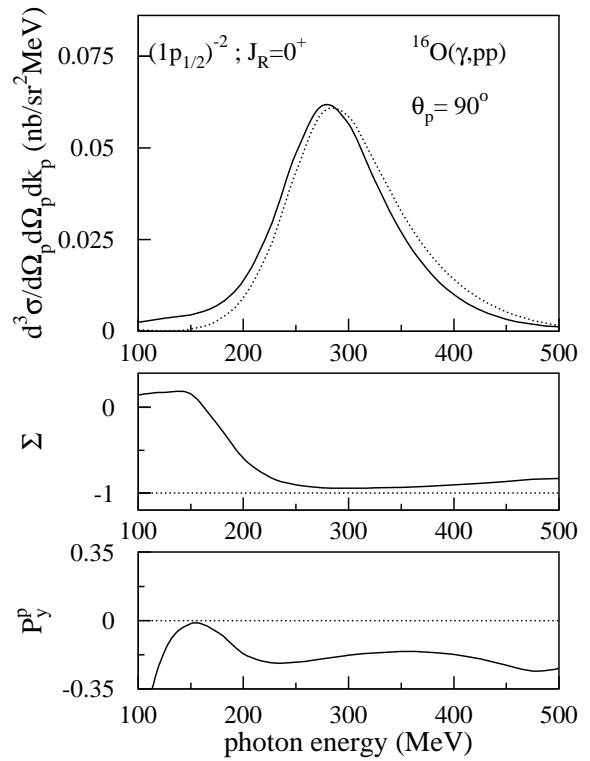
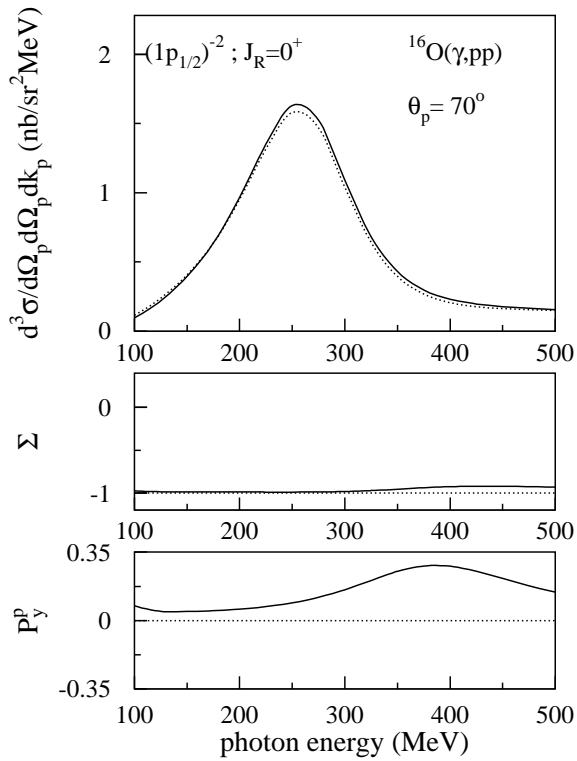
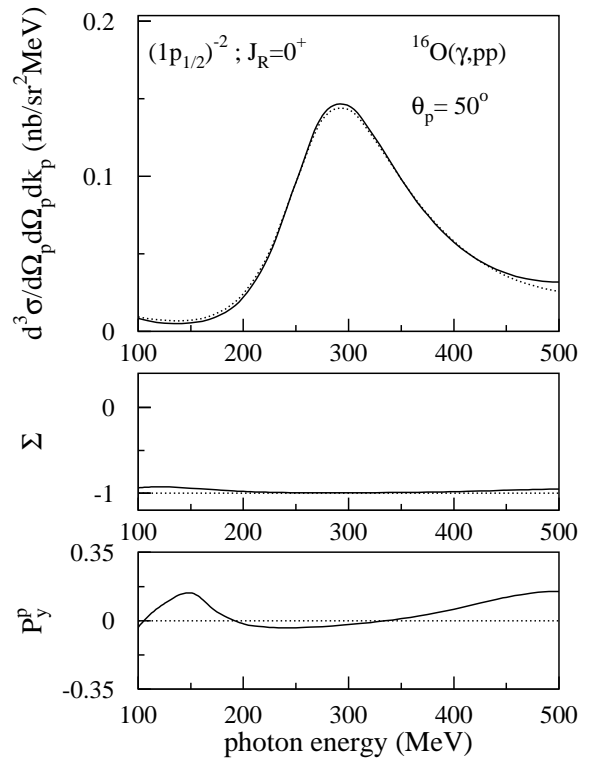
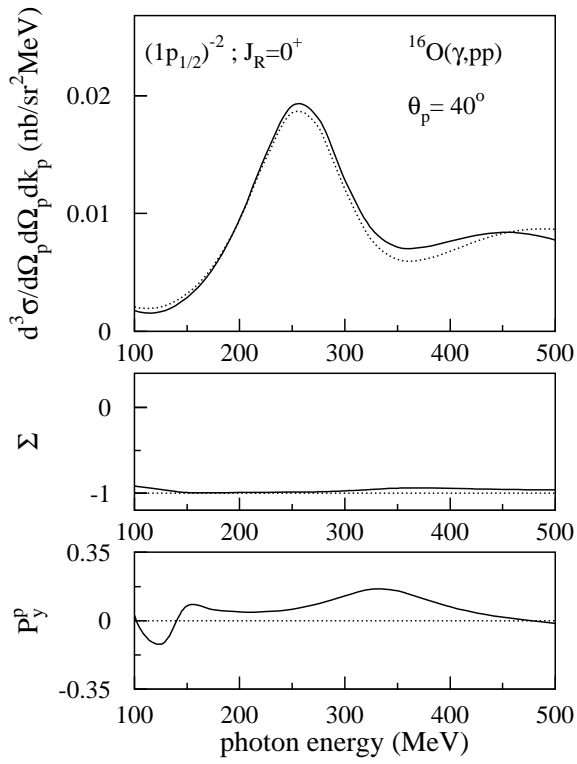


Figure 10

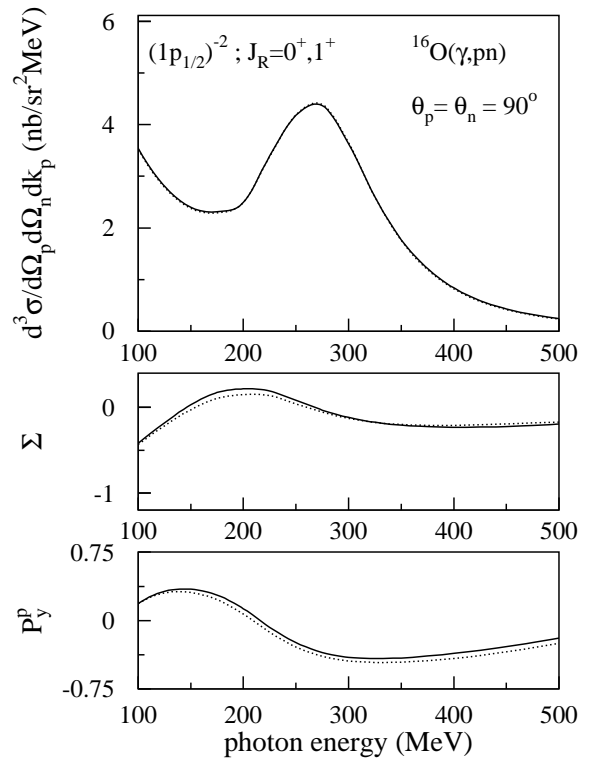
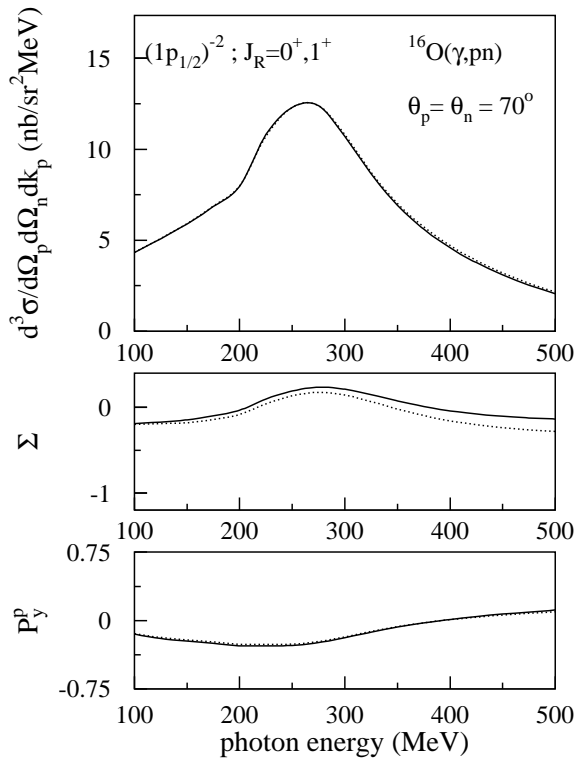
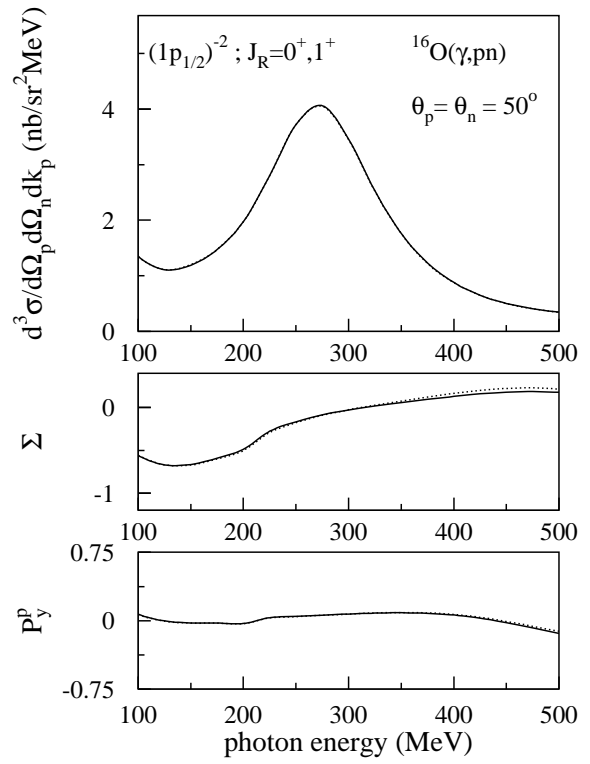
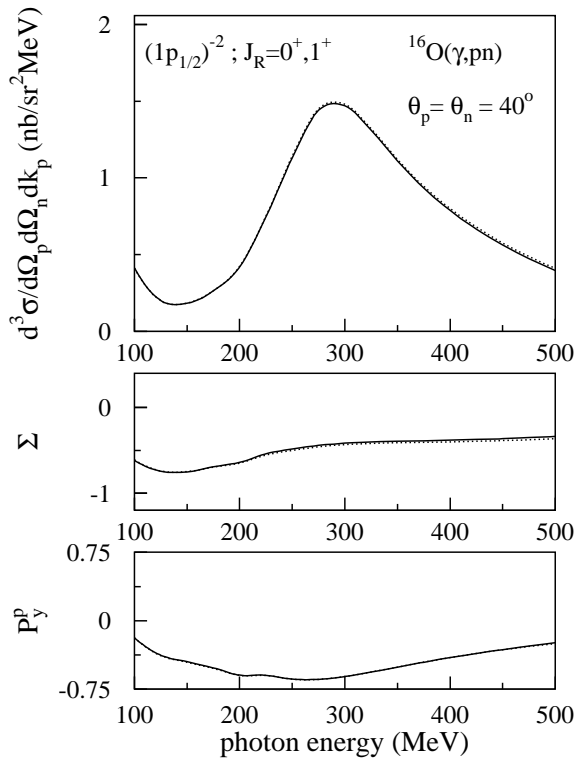


Figure 11